Geoscience Frontiers 10 (2019) 973–988

HOSTED BY

Contents lists available at ScienceDirect

China University of Geosciences (Beijing)

Geoscience Frontiers

journal homepage: www.elsevier.com/locate/gsf

Research Paper

Tectonic evolution of the West Kunlun Orogenic Belt along the northern margin of the Tibetan Plateau: Implications for the assembly of the Tarim terrane to Gondwana

Chuan-Lin Zhang [a,*], Hai-Bo Zou [b], Xian-Tao Ye [a], Xiang-Yan Chen [a]

[a] College of Oceanography, Hohai University, Nanjing 210093, China
[b] Department of Geosciences, Auburn University, Auburn, AL 36849-5305, USA

ARTICLE INFO

Article history:
Received 9 November 2017
Received in revised form
3 April 2018
Accepted 11 May 2018
Available online 2 June 2018
Handling Editor: Sanzhong Li

Keywords:
West Kunlun Orogenic Belt
Tectonic unit
Metamorphic basement
Zircon and monazite U-Pb dating
Tectonic evolution

ABSTRACT

The West Kunlun orogenic belt (WKOB) along the northern margin of the Tibetan Plateau is important for understanding the evolution of the Proto- and Paleo-Tethys oceans. Previous investigations have focused on the igneous rocks and ophiolites distributed mostly along the Xinjiang-Tibet road and the China-Pakistan road, and have constructed a preliminary tectonic model for this orogenic belt. However, few studies have focused on the so-called Precambrian basement in this area. As a result, the tectonic affinity of the individual terranes of the WKOB and their detailed evolution process are uncertain. Here we report new field observations, zircon and monazite U-Pb ages of the "Precambrian basement" of the South Kunlun terrane (SKT) and the Tianshuihai terrane (TSHT), two major terranes in the WKOB. Based on new zircon U-Pb age data, the amphibolite-facies metamorphosed volcano-sedimentary sequence within SKT was deposited during the late Neoproterozoic to Cambrian (600–500 Ma), and the flysch-affinity Tianshuihai Group, as the basement of the TSHT, was deposited during the late Neoproterozoic rather than Mesoproterozoic. The rock association of the volcano-sedimentary sequence within SKT suggests a large early Paleozoic accretionary wedge formed by the long-term low-angle southward subduction of the Proto-Tethys Ocean between Tarim and TSHT. The amphibolite-facies metamorphism in SKT occurred at ca. 440 Ma. This ca. 440 Ma metamorphism is genetically related to the closure of the Proto-Tethys Ocean between Tarim and the Tianshuihai terrane, which led to the assembly of Tarim to Eastern Gondwana and the final formation of the Gondwana. Since the late Paleozoic to early Mesozoic, the northward subduction of the Paleo-Tethys Ocean along the Hongshihu-Qiaoertianshan belt produced the voluminous early Mesozoic arc-signature granites along the southern part of NKT-TSHT. The Paleo-Tethys ocean between TSHT and Karakorum closed at ca. 200 Ma, as demonstrated by the monazite age of the paragneiss in the Kangxiwa Group. Our study does not favor the existence of a Precambrian basement in SKT.

© 2018, China University of Geosciences (Beijing) and Peking University. Production and hosting by Elsevier B.V. This is an open access article under the CC BY-NC-ND license (http://creativecommons.org/licenses/by-nc-nd/4.0/).

1. Introduction

The West Kunlun Orogenic Belt (WKOB) is bounded by the Tarim Basin to the north, the Tibetan Plateau to the south, and the Pamir Plateau to the west (Yin and Harrison, 2000; Gibbons et al., 2015). WKOB is offset from the East Kunlun Orogen and the Songpan-Ganzi terrane by the Altyn sinistral strike-slip fault to the east (Fig. 1a). As one of the major tectonic units of the Tibetan Plateau and the central orogenic belt in China (*i.e.*, the West Kunlun-Eastern Kunlun-Qilian-Qinling-Dabie orogen, see Dewey et al., 1988; Jiang et al., 1992), WKOB is important for understanding the evolution of the Proto- to Paleo-Tethys Ocean. Nevertheless, fundamental geological data and knowledge of the tectonic evolution of the WKOB are limited due to access difficulty and harsh natural conditions before 1990s. Studies on the WKOB since 1990s (e.g., Pan, 1990, 1993, 1996; Matte et al., 1992, 1996; Pan and Wang, 1994; Mattern et al., 1996; Yang et al., 1996; Xiao et al., 1998; Mattern and Schneider, 2000; Yin and Harrison, 2000) have provided new insights on the tectonic evolution of the WKOB (e.g., Yuan, 1999;

* Corresponding author. Fax: +86 25 83786641.
E-mail address: zhangchuanlin@hhu.edu.cn (C.-L. Zhang).
Peer-review under responsibility of China University of Geosciences (Beijing).

https://doi.org/10.1016/j.gsf.2018.05.006
1674-9871/© 2018, China University of Geosciences (Beijing) and Peking University. Production and hosting by Elsevier B.V. This is an open access article under the CC BY-NC-ND license (http://creativecommons.org/licenses/by-nc-nd/4.0/).

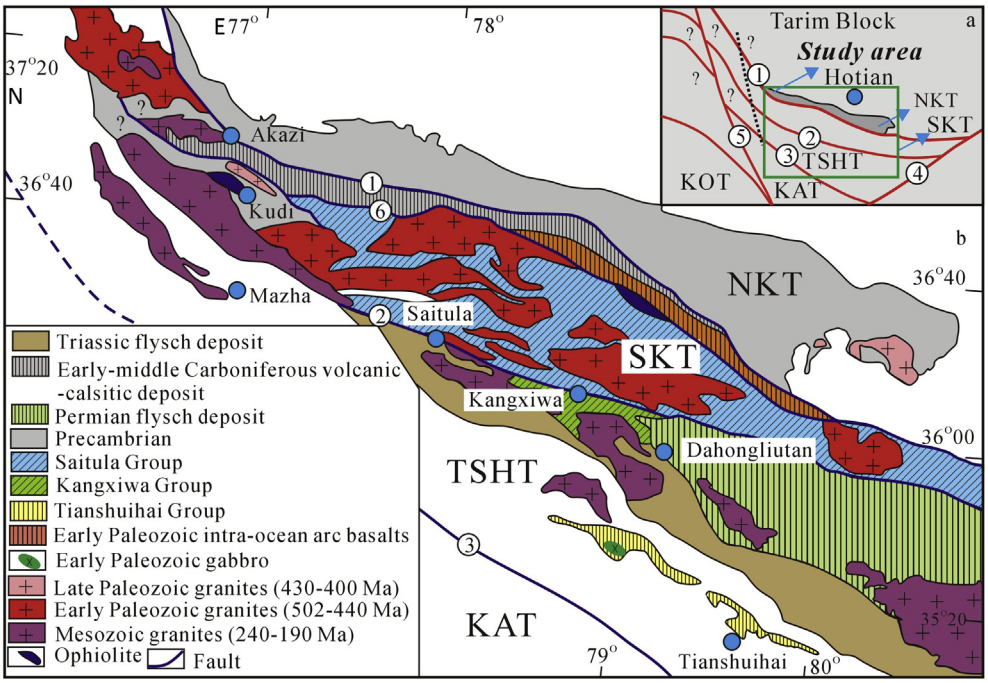

Figure 1. (a) Tectonic framework of the West Kunlun orogenic belt (WKOB) and its adjacent areas showing the main tectonic units of the WKOB. The dashed line represents the boundary between the two distinct segments of the WKOB as deduced from their individual aeromagnetic anomaly and recent studies (see Ji et al., 2004); (b) sketch geological map of the eastern section of the WKOB (see details in the text). The faults marked in (a) and (b): ① the Kegang-Akazi fault, ② the Kangxiwa fault, ③ the Qianertianshan–Hongshanhu fault, ④ the Altyn fault, ⑤ the Tashikoergan fault, ⑥ the Talong fault.

Jiang et al., 2002, 2005, 2008, 2013; Wang et al., 2002, 2004; Xiao et al., 2002a, b, 2005; Yuan et al., 2002, 2004, 2005; Ducea et al., 2003; Wang, 2004; Zhang et al., 2006a, 2007a). Most geologists favor the notion that the southward subduction of the Proto-Tethys Ocean beneath the South Kunlun Terrane (SKT) since Sinian led to the closing of this ocean basin and the amalgamation of the North Kunlun Terrane (NKT) and SKT during the Early Paleozoic, with only the remnants of the Proto-Tethys oceanic crust being preserved along the Qytag-Kudi suture zone (Pan, 1996; Xiao et al., 1998; Mattern and Schneider, 2000; Jiang et al., 2002). During the late Paleozoic to mid-Mesozoic, the southerly located Paleo-Tethys Ocean was consumed beneath the SKT and produced a Late-Carboniferous to mid-Jurassic magmatic arc in the southern SKT and the Tianshuihai Terrane (TSHT). Arc magmatism affected the southern SKT and the large Karakorum accretionary prism which formed as a result of the consumption of the Paleo-Tethys ocean (Mattern and Schneider, 2000; Zhang et al., 2016a). The dextral shear sense of ductile faults parallel to the South Kunlun/Karakorum boundary, suggests oblique plate convergence with a dextral component during the early to middle Jurassic (Mattern and Schneider, 2000).

Previous studies have focused on the igneous rocks and some major geological units such as the ophiolites along the Xingjiang-Tibet road and the China-Pakistan road (e.g., Xu et al., 1994; Yang et al., 1996; Zhang et al., 1996; Mattern and Schneider, 2000; Zhou et al., 2000; Wang et al., 2002; Zhang et al., 2004; Mahar et al., 2014; Liu and Wang, 2016). Few scientists have studied the widely distributed so-called Precambrian basement in WKOB (Zhang et al., 2007a). In addition, the orientation and the process of oceanic crust subduction, the timing of the closing of the Proto- and Paleo-Tethys oceans, and the final formation of the WKOB, remain to be determined.

In recent years, local geologists have completed 1/250,000 geological mapping of the WKOB which have significantly improved our geologic knowledge of the WKOB (Han et al., 2001, 2002, 2004; Ji et al., 2004; Cui et al., 2006a,b, 2007a). Based on these data, we revisit this major orogenic belt for a better understanding of the tectonic evolution of the Tibetan Plateau. In this contribution, we report our new field observations and zircon and monazite U-Pb ages for the metamorphic rocks from the so-called Precambrian basement in the eastern section of the WKOB. The aims of this study are to: (a) determine the ages and their tectonic attribution of the so-called Precambrian basement, (b) decipher the coupling relationship between oceanic crust subduction, terrane accretion, metamorphism and igneous activities, and (c) construct a more accurate model for the tectonic evolution of the WKOB.

2. Regional geology

2.1. Tectonic framework of the West Kunlun

The West Kunlun is tectono-stratigraphically subdivided into three main units: the North Kunlun Terrane (NKT) (also termed as the southern margin of the Tarim Block, the Tiekelike uplift in literature, e.g., Xinjiang BGMR, 1993; Pan, 1996; Zhang et al., 2003), the narrow South Kunlun Terrane (SKT), and the Tianshuihai Terrane, also known as Uygur Terrane (TSHT, e.g., Mattern and Schneider, 2000) (Fig. 1a). NKT and SKT are separated by the ophiolite-bearing Kudi-Qimanyute suture (Fig. 1b). It was believed that this suture zone extended toward northwest to Oytagh, based on the presence of the Oytagh plagiogranite (Jiang et al., 2002). However, recent studies have revealed that the Oytagh plagiogranite emplaced at ca. 330 Ma and thus is not a member of the early Paleozoic ophiolite complex between NKT and SKT (Zhang et al., 2006; Jiang et al., 2008). Thus, the orientation of the suture zone between NKT and SKT is still unclear. The Kangxiwa fault was regarded as the suture zone between SKT and TSHT, which trends E–W in the eastern section of the WKOB. To the west, some geologists suggested that it was switched off by the Cenozoic N-S-trending Tashikoergan fault (Jiang et al., 2013; Zhang et al., 2016a).

Recent studies have revealed clear differences between the western and eastern sections of the WKOB (Robinson et al., 2004, 2007, 2016; Zhang et al., 2007a, 2018a; Ji et al., 2011). This conclusion is also supported by the pronounced difference in the regional geophysical field between the two segments (Matte et al., 1996; Yuan, 1996; Gao et al., 2000). A NNW extending strike-slip fault can divide the WKOB into western and eastern parts on the basis of the aeromagnetic anomaly features, but we know little about this fault due to access difficulty (marked as dashed line in Fig. 1a). This study focuses on the eastern section of the WKOB (Fig. 1b).

2.2. The North Kunlun Terrane (NKT)

NKT is an uplifted terrane of the Tarim block (Zhang et al., 2013). The major Precambrian rock series of NKT are mainly composed of the Paleoproterozoic Heluositan complex (2.34–2.41 Ga, Zhang et al., 2007b; Wang et al., 2014; Ye et al., 2016) (Fig. 2a), the Mesoproterozoic greenschist- to amphibolite-facies metamorphosed and intensively folded sedimentary sequences (the Kalakashi Group), the mid-Neoproterozoic greenschist-facies metamorphosed and folded volcanic-sedimentary sequences, and the late Neoproterozoic unmetamorphosed carbonate-clastic-tillite sequences (see details in Zhang et al., 2016b) (Fig. 2a). The Mesoproterozoic to late Neoproterozoic tectonostratigraphic features revealed the assemblage and breakup process of NKT during the evolution of the Rodinia supercontinent (Xu et al., 2013; Zhang et al., 2016b). The ca. 1.0 Ga metamorphic age of the Kalakashi Group may be related the assembly of the Tarim to the Rodinia supercontinent (Zhang et al., 2003). In NKT, Devonian red molasse unconformably overlies the broadly folded, unmetamorphosed Neoproterozoic–Cambrian rocks and the tightly-folded, amphibolite-facies metamorphic Mesoproterozoic rocks, and subsequently is overlain by the Carboniferous–Permian shallow marine carbonate. The coal-bearing upper Triassic-Cenozoic molasse sedimentary sequence unconformably overlying on the late Paleozoic rocks was the far away effects of the closing of the Paleo-Tethys ocean (Mattern and Schneider, 2000; Yin and Harrison, 2000).

2.3. The South Kunlun Terrane (SKT)

SKT was often regarded as a drifted Precambrian terrane from the southern margin of the Tarim Block during the late Neoproterozoic to Sinian and shares a common Precambrian basement with NKT (Pan, 1996; Wang, 2004; Wang et al., 2004). According to the latest 1/250,000 geological mappings (Han et al., 2001, 2004; Cui et al., 2007a, b), the so-called Precambrian basement was termed as Mesoproterozoic Saitula Group in northern SKT and as the Kangxiwa Group in southern SKT (Fig. 1b). Both groups are composed primarily of schist and gneiss locally intercalated with amphibolite layers (see the following discussions). The overlying strata are dominated by the Upper Paleozoic to Mesozoic siliciclastic-, carbonate- and calc-alkaline volcanic rocks (Pan, 1993; Pan and Wang, 1994). Voluminous granites intruded the "Precambrian basement" during (1) the early Paleozoic and (2) the late Paleozoic to early Mesozoic (Yin and Bian, 1995; Xu et al., 1996; Zhang et al., 2005; Cui et al., 2006c; Jiang et al., 2013; Liu et al., 2015) (Fig. 2).

2.4. The Tianshuihai Terrane (TSHT)

TSHT is a NW–SE trending belt between the Mazha–Kangxiwa fault (#2 fault in Fig. 1b) to the north and the Qianertianshan–Hongshanhu fault to the south (#3 fault in Fig. 1b). Knowledge of TSHT geology is highly incomplete due to geographic remoteness and widespread glacial coverage (Cui et al., 2006c; Zhang et al., 2008). Xiao et al. (2005) and Liu et al. (2015) suggested that TSHT is the western extension of the Songpan–Ganzi block which collided with SKT during the Early Mesozoic. However, Yuan et al. (2002) and Zhang et al. (2007a) proposed that TSHT was a part of SKT.

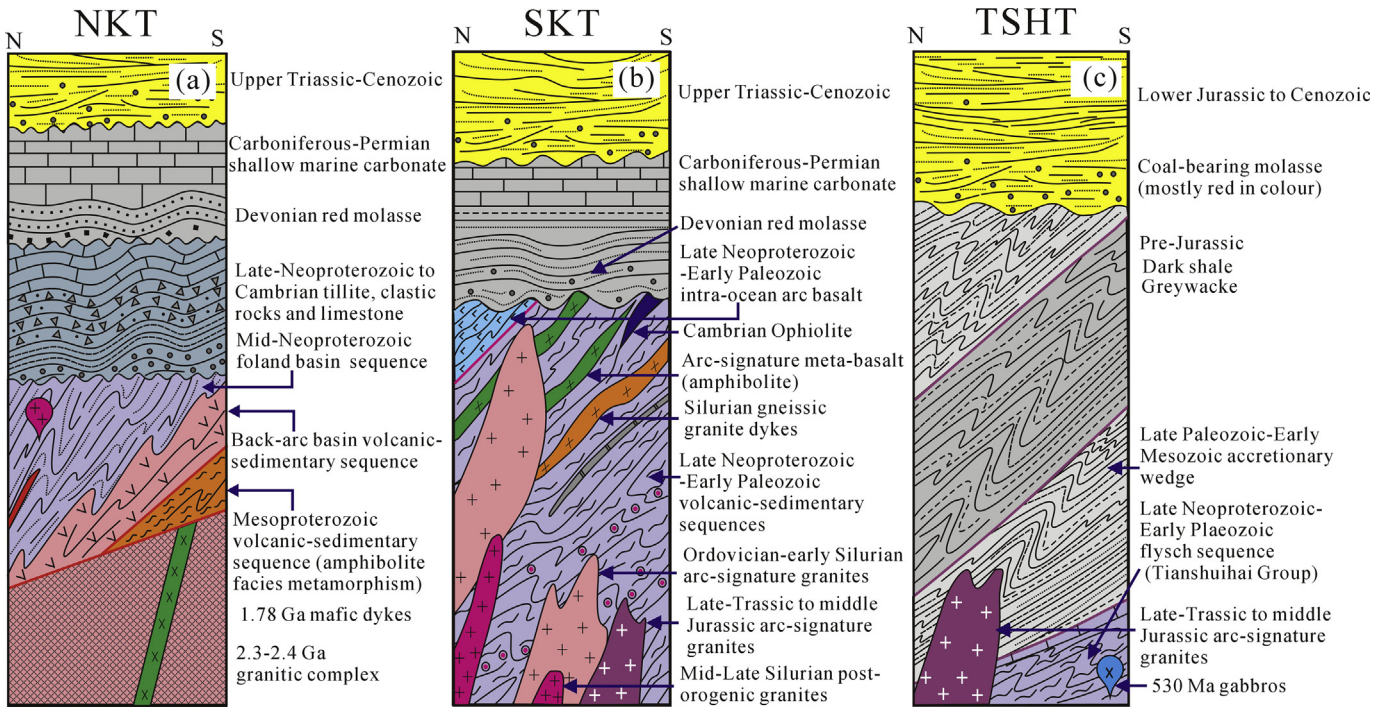

Figure 2. Juxtaposition of the stratigraphy of the Northern Kunlun terrane (NKT), Southern Kunlun terrane (SKT) and the Tianshuihai terrane (TSHT). Note the similar development in NKT and SKT occurs during the Devonian and the similar development in SKT and TSHT occurs during the Mesozoic (modified after Mattern and Schneider, 2000).

The Precambrian member in TSHT is termed as the Tianshuihai Group. This group mainly consists of meta-greywackes and limestone and is in fault or unconformable contact with the late-Paleozoic to early Mesozoic accretionary wedge (Fig. 2c). The thick monotonous and partly metamorphosed successions of clastic marine deposits exhibit a flyschoid character (Mattern and Schneider, 2000).

3. Field observations and sample description

The metamorphic rocks in the eastern section of SKT were termed as the Kangxiwa Group in southern SKT and as the Saitula Group in northern SKT (Fig. 1b). The Saitula Group is in fault contact with the late Paleozoic back-arc basin sequences and the early Paleozoic low greenschist-facies metamorphic Taxidaban Group. Late Cambrian to early Ordovician ophiolite relics tectonically intermingled in the northern margin of the Saitula Group (Fig. 1b). Previous works demonstrated that this ophiolite belt was thrust from north to south after the closing of the Proto-Tethys ocean (Zhou et al., 1999; Li and Zhang, 2014). On the south side, the Saitula group is in fault contact with the late Paleozoic to early Mesozoic flysch and the Kangxiwa Group by the sinistral strike-slip Kangxiwa fault (Fig. 1b). Similar with the scenario of NKT, Devonian red molasse unconformably overlies the Saitula Group (Fig. 2). N–S cross section observations show that the schistosity and the stratification are parallel to each other in most places and dip to north with the dip angle varying from 75° to 45° from north to south. The 1:250,000 mapping revealed that voluminous early Paleozoic granites (mostly in the northern part) and some early Mesozoic granites (mostly along the southern part) intruded into the Saitula Group (Fig. 1b). At several outcrops, granite-granodiorite gneiss sheets 1–2 m thick, intrude the Saitula Group. In line with our field observations and previous studies (Xinjiang BGMR, 1993; Cui et al., 2006a; Zhang et al., 2007a), the Saitula Group is mainly composed of gneiss-schist and layers or lens of amphibolite with minor marble at the top of this group (the marble member was termed as the Sangzhutage Group in the early literature, e.g., Xinjiang BGMR, 1993). At several outcrops, amphibolite and biotite plagioclase-quartz granofels, with variable thickness, interbedded with each other (Fig. 3a and b). However, in one locality (northeast of Saitula town) the amphibolite occurs as a pluton ca. 2500 m long and 500–1500 m wide in the gneiss-schist and shares common foliation with the wall rocks (Fig. 3c). We infer that the amphibolite was a mafic intrusive pluton and underwent similar tectonic events after its emplacement. The layered amphibolites (or amphibolite gneiss) in the gneiss-schist are fine- to medium-grained, exhibit gneissic structure, and comprise mainly plagioclase (40%–50%), hornblende (40%–50%), biotite (5%–10%) with occasional quartz (1%–5%) and Fe-Ti oxides (3%–10%). Some hornblende was replaced by chlorite (Fig. 4a). Apatite and zircon occur as accessory

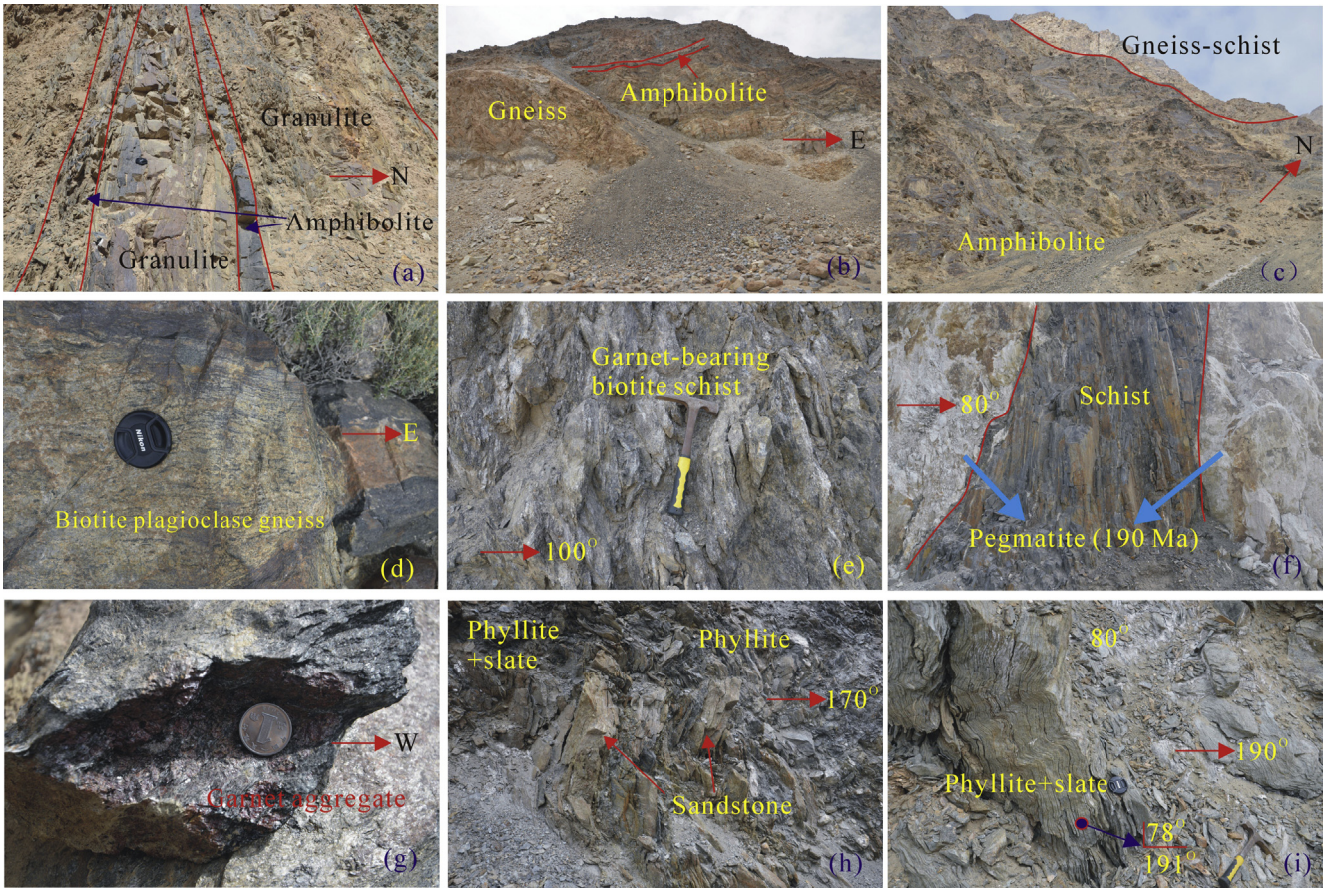

Figure 3. Representative field photographs of the studied metamorphic sequences in SKT and TSHT. (a, b) The interlayer structure of the amphibolite and the granofels from Saitula Group, indicating the precursor of the amphibolite was most likely basalt or mafic sheet; (c) the amphibolite occurs as a pluton (with ca. 2500 m in length and 500–1500 m in width) in the gneiss-schist, its precursor was likely a mafic intrusion; (d) the hornblende-bearing gneiss from the Saitula Group, its precursor was likely rhyolite; (e) garnet-bearing biotite schist from the Kangxiwa Group, the bedding was completely replaced by foliation; (f) biotite schist intruded by the deformed pegmatite dykes, monazite U-Pb dating revealed the pegmatite emplaced at 209 Ma; (g) garnet biotite schist from the Kangxiwa Group, and some garnet aggregate is seen at outcrops; (h) the sandstone layer in the phyllite and slate from the Tianshuihai Group; (i) phyllite and slate in the Tianshuihai Group, foliation was parallel with the bedding plane.

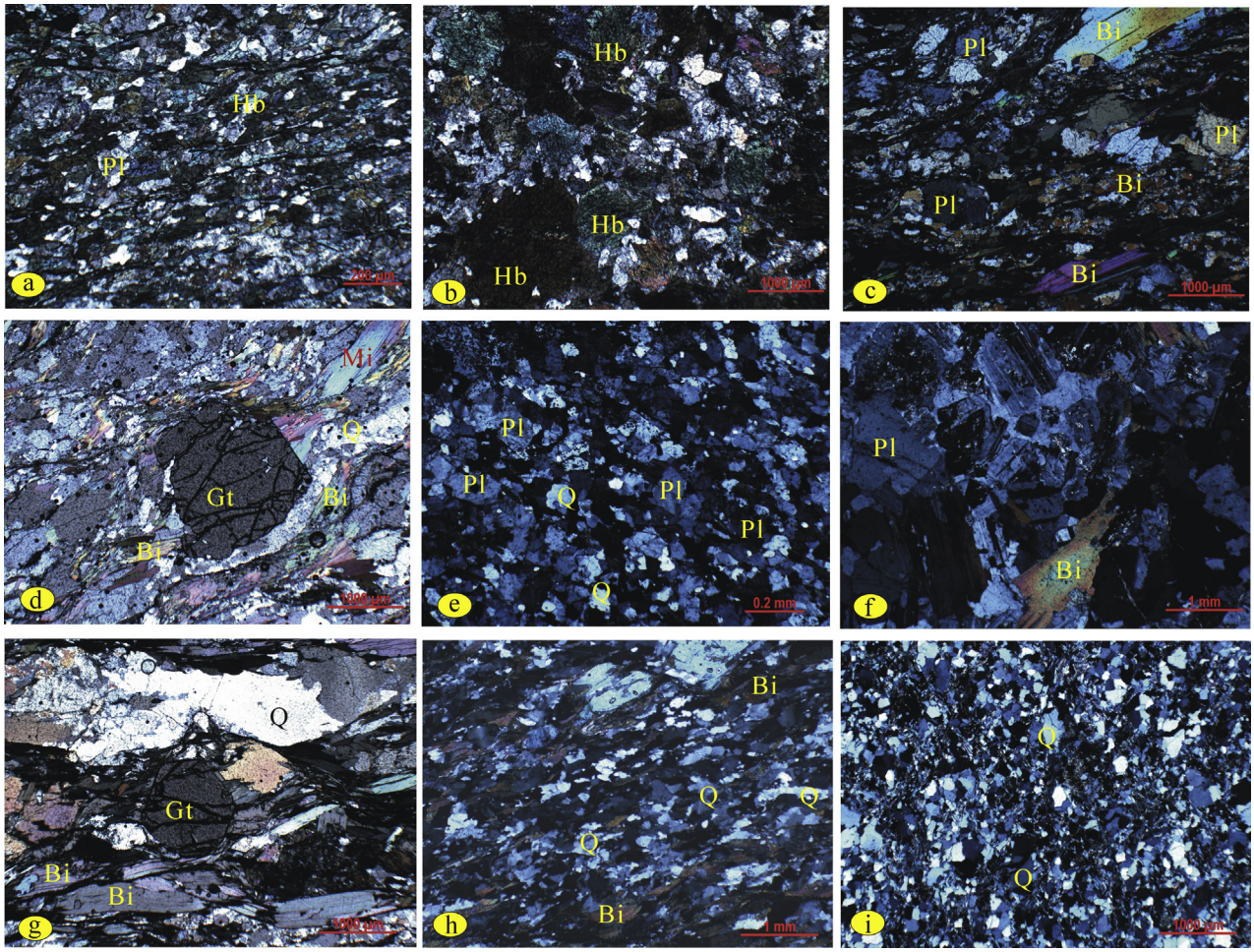

Figure 4. Photomicrographs of the representative rocks for zircon and monazite U-Pb age analysis from the Saitula Group, Kangxiwa Group and Tianshuihai Group. (a) Fine-grained plagioclase-amphibolite gneiss layer from the Saitula Group (see Fig. 3a, sample 2015D012); (b) altered gabbro intrusion in the Saitula Group (sample 2015D018); (c) biotite plagioclase gneiss from the Saitula Group (sample 2015D008); (d) garnet bearing gneiss (sample 2015D12-2); (e) quartz plagioclase granofels from the Saitula Group (sample 2015D015); (f) gneissic granodiorite (sample 2015D016); (g) garnet biotite schist from the Kangxiwa Group (sample 2015D005-2); (h) biotite quartz schist; (i) quartz sandstone from the Tianshuihai Group (sample 2015D001) (see details in the text). Abbreviations: Bi—biotite, Gt—garnet, Q—quartz, Pl—plagioclase, Hb—Hornblende.

minerals. Based on the mineral assemblage, and in combination with their layered structure observed in the field, we infer that their protoliths are probably basalt or mafic sheets, indicating that they were coeval with the gneiss-schist association. The amphibolite occurring as a pluton is of coarse-grained, and is composed mainly of hornblende (50%–60%), plagioclase (20%–30%), Fe-Ti oxides (2%–5%) and minor quartz (less than 1%) (Fig. 4b). Some hornblende grains could be replacement product of clinopyroxene according to their clinopyroxene pseudomorph (Fig. 4b). The Saitula Group include biotite plagioclase gneiss, garnet-bearing schist and gneiss, and biotite schist, and have variable contents of biotite (5%–30%), quartz (15%–45%), plagioclase (10%–40%), garnet (1%–15%), and amphibole (1%–10%). According to the mineral assemblage and texture, most of the gneisses are metamorphosed from clastic rocks involved with variable volcanic debris, whereas the garnet-bearing schist and gneiss might have been metamorphosed from clastic protoliths, judging from the presence of highly aluminous minerals in these rocks (Fig. 4c and d). Granofels layers were observed in the gneiss-schist and are mainly composed of plagioclase (50%–60%, including some microcline) and quartz (35%–45%) with minor biotite (1%–5%). In line with mineral composition, we infer that its precursor is most likely rhyolite or granitic sheets (Fig. 4e). Deformed granite-granodiorite dykes are composed of 30%–40% plagioclases, 15%–25% perthite, 20%–30% quartz, 5%–10% biotite and accessory minerals, such as zircon, apatite and ilmenite. In thin sections, some fine-grained felsic aggregates and the variable degree of foliation structure indicate dynamic metamorphism after their emplacement (Fig. 4f).

The Kangxiwa Group mainly consists of diverse schist and gneiss, including the garnet (bearing) biotite schist, two-mica quartz schist, sillimanite-garnet-biotite schist or gneiss, and garnet-bearing gneiss (Fig. 3e). Strongly deformed felsic pegmatites are occasionally seen on the outcrops (Fig. 3f). The paragneisses are of medium- to coarse-grained foliated phaneritic texture and/or porphyritic phaneritic texture, and gneissic or schistose structure (Fig. 4g and h). Main minerals include sillimanite (1%–10%), diopside (little to 1%), garnet (1%–20%, some up to 50%, as phenocryst Fig. 3c), biotite (10%–25%), muscovite (1%–10%), quartz (20%–40%), plagioclase (1%–5%, some up to 15%), and potassium feldspar (1%–5%). At several outcrops, garnet aggregates are seen (Fig. 3g).

The Tianshuihai Group was considered as the early Mesoproterozoic basement of TSHT (Xinjiang et al., 1993). This group is mainly composed of clastic rocks with minor limestone and underwent low greenschist facies metamorphism and tightly folded deformation (Fig. 3h and i). The Tianshuihai Group was unconformably covered by the late Paleozoic flysch deposit and intruded by the ca. 530 Ma gabbro and Mesozoic granites (Hu

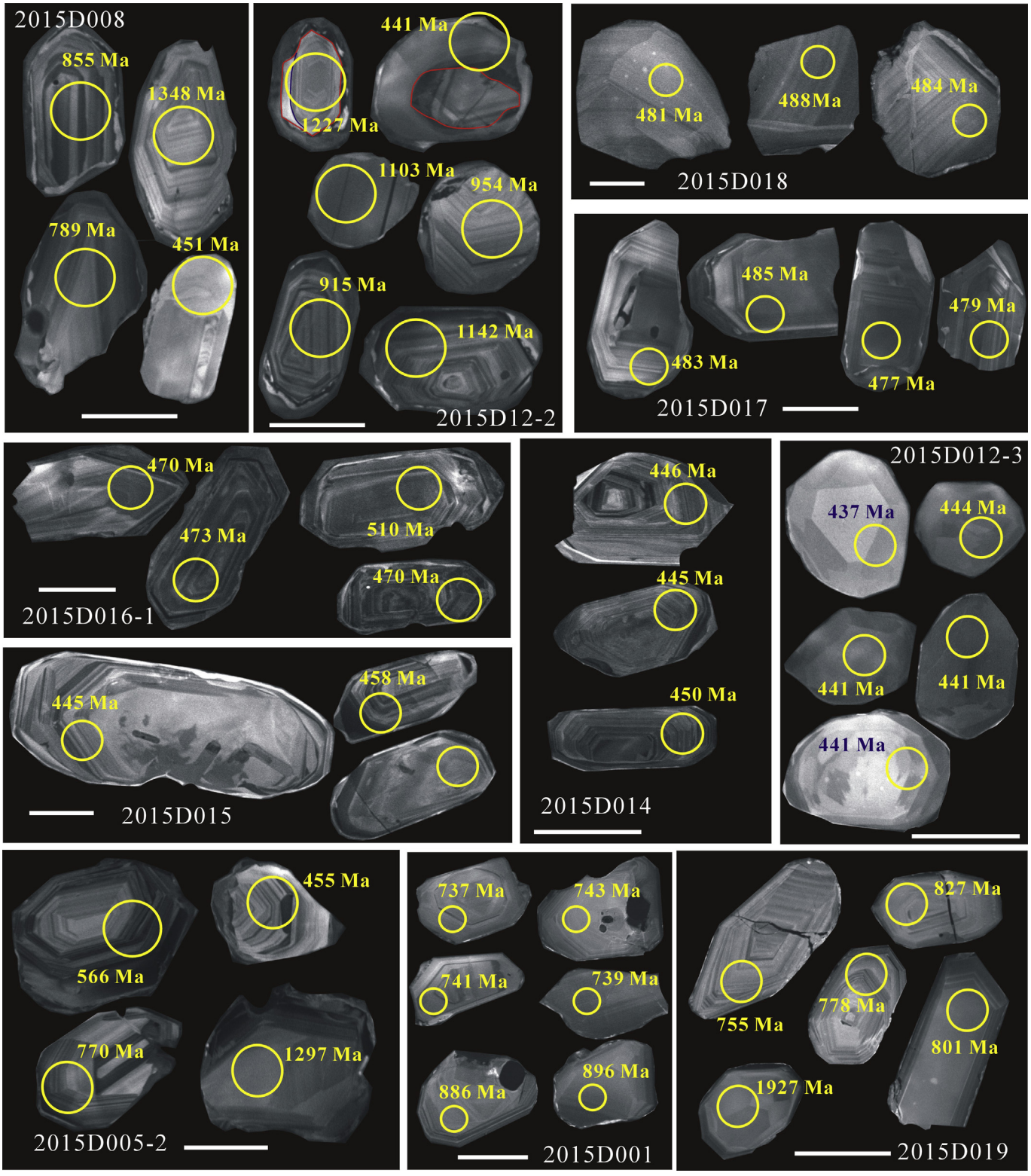

Figure 5. Representative cathodoluminescene images of the zircons from the representative rocks from the Saitula Group, the Kangxiwa Group and the Tianshuihai Group (see details in the text). The scale bar is 50 μm.

et al., 2016). In line with field observations, the main rocks include sericite-chlorite (quartz) schist, siltstone, fine-grained sandstone and plagioclase-quartz greywacke (Fig. 4h and i). Low greenschist facies metamorphic minerals such as biotite, sericite and chlorite are commonly seen in most rock types. Hu et al. (2016) reported 480–530 Ma granite and gabbro intruding into the Tianshuihai Group, which provided a minimum deposition age. Due to its tight folding, the precise thickness of the Tianshuihai Group sedimentary sequence is unknown (Xinjiang BGMR, 1993; Hu et al., 2016).

Seven geochronological samples were collected from the Saitula Group. The rock types include garnet biotite quartz schist (gneiss), ganofels, amphibolite and gneissic granitic dykes within the gneiss-schist. Two samples from two individual granodiorite plutons intruding the Saitula Group were collected for zircon U-Pb and Hf isotope analysis. Sample locations and rock types are given in Supplementary Table 1. Three samples were collected from the Kangxiwa Group. Sample 2015D005-2 and 2015D005-3 are garnet plagioclase gneiss and garnet biotite schist at the same location. Sample 2015D010 was collected from a deformed leucogranite dyke intruding the Kangxiwa Group. Sample 2015D001 and sample 2015D019 collected from the Tianshuihai Group are sandstone samples from a layer within the phyllite, composed of quartz (70%–80%), plagioclase (10%–20%), debris (5%–10%), opaque mineral (pyrite and Fe-Ti oxides), chlorite (less than 5%) and sericite (less than 5%) (Fig. 4i). Locations of the samples from the Kangxiwa Group and the Tianshuihai Group are given in Supplementary Table 1.

4. Analytical procedures

Zircon and monazite separations were carried out using conventional magnetic and density techniques to concentrate non-magnetic, heavy fractions. Zircon and monazite grains were then hand-picked under a binocular microscope. For the zircon U-Pb dating, the grains and zircon standard 91500 were mounted in epoxy mounts that were subsequently polished to section the crystals in half for analysis. All zircons were documented with transmitted and reflected light micrographs as well as Cathodoluminescence (CL) images to reveal their internal structures. Zircon U-Pb ages were analyzed using the LA-ICPMS method at the Tianjin Institute of Geology and Mineral Resources, Chinese Geology Survey (CGS). A Neptune MC-ICP-MS coupled with a 193 nm excimer laser ablation system was used to determine zircon U-Pb ages. The laser beam diameter was 35 μm and it was operated with a frequency of 10 Hz. Every set of five sample analyses was followed by analysis of the zircon standards 91500 and eight sample analyses followed by the zircon standard GJ-1 (Jackson et al., 2004), and the glass standard NIST610 (Hou et al., 2009; Geng et al., 2011). Common Pb was corrected using the method proposed by Andersen (2002). The U-Pb concordia plots were processed with ISOPLOT 3.0 and data are presented with 1σ errors and 95% confidence limits (Ludwig, 2003). The zircon U-Pb age data are reported in Supplementary Table 2.

For the monazite U-Pb dating, monazite grains and the monazite standard 44069 (Wan et al., 2004) were mounted in epoxy mounts. The mounts were subsequently polished to section the crystals almost in half. All the monazite grains were documented with BSE images to reveal their inner structures. Monazite U-Pb ages were determined using the LA-ICPMS method at the same laboratory with the same instrument at the Tianjin Institute of Geology and Mineral Resources. Detailed analytical procedures have been reported in Cui et al. (2012). Monazite U-Pb analytical results are given in Supplementary Table 3.

The zircon Lu-Hf isotope measurements were performed at the Tianjin Institute of Geology and Mineral Resources, mostly on the ablated spots where U-Pb analysis was made. The analytical procedure has been documented in Wu et al. (2006) and Geng et al. (2011). The isotope data are presented in Supplementary Table 4.

5. Analytical results

5.1. Zircon and monazite U-Pb ages of the Saitula Group

Zircons from the two paragneiss samples (2015D008, 2015D012-2) are similar in size and shape. These zircons are 50–150 μm long with length/width ratios of 1–3, and some zircons are rounded or ovoid in shape. Zircon CL images show distinctive features (Fig. 5). Some zircons exhibit oscillatory zoning, similar to that of the zircons crystallized from silicic magma, whereas others show homogenous or wide striped inner structure, sharing some features of the zircons crystallized from mafic magma. The distinct features of the detrital zircons suggest that they were derived from different sources. Core-mantle structure is commonly seen in CL images but some mantles are too thin for a spot analysis. Most mantles are homogeneous and dark grayish in CL images (Fig. 5), indicating their high Th and U contents and their possible rapid crystallization in a relatively short time (Vavra et al., 1999; Whitehouse and Kamber, 2002). Twenty-six and forty-one analyses were conducted for sample 2015D008 and 2015D012-2, respectively. The results show variable Th and U contents and Th/U ratios (mostly higher than 0.4, Supplementary Table 1). Most analyses on detrital zircons yield concordant ages ranging from 2500 Ma to 600 Ma whereas others show variable degrees of loss of radiogenic Pb (Fig. 6a). Eight analyses were conducted on the mantle parts of the zircons showing core-mantle structure. Though we tried to carefully avoid the cores during laser ablation, some analyses could be affected by the cores (see following discussions).

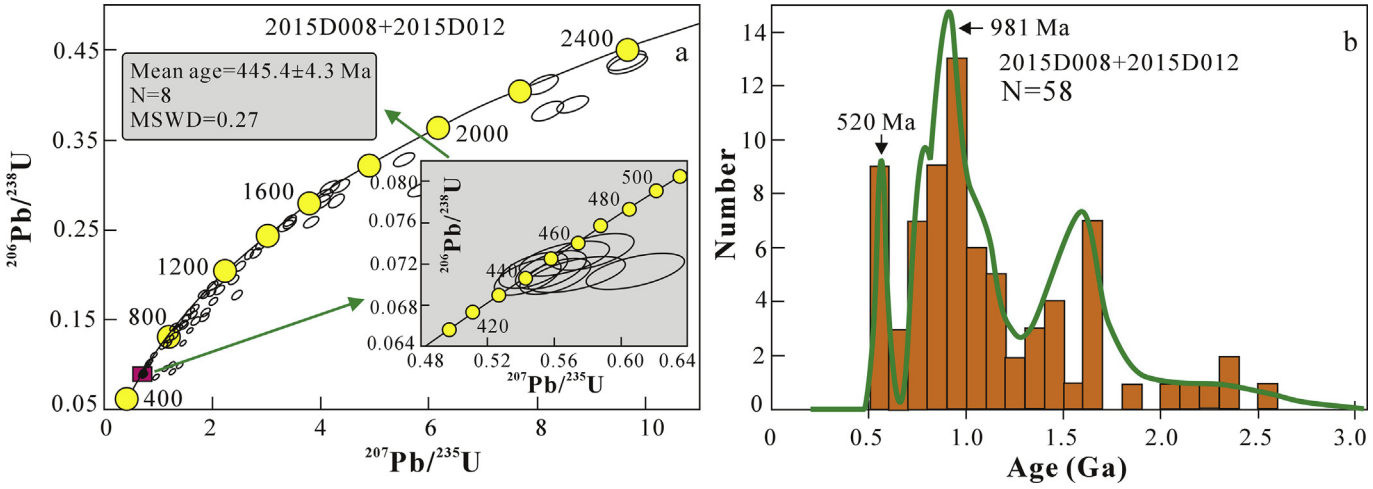

Figure 6. Concordia and the histogram of $^{206}Pb/^{238}U$ ages of the detrital zircons of the paragneiss samples from the Saitula Group (see details in the text).

Nevertheless, the eight analyses yield concordant ages with a weighted mean age of 445 ± 6.3 Ma (MSWD = 0.27) (see inset of Fig. 6a). Excluding the spots showing significant radiogenic lead loss, as shown in Fig. 6b, the $^{206}Pb/^{238}U$ ages of the detrital zircons from the two paragneiss samples exhibit major age peaks at ca. 520 Ma, 980 Ma and 1600 Ma.

Zircons from the altered gabbro sample (2015D018, Fig. 4b) are subhedral to anhedral and are 80–150 μm long with length to width ratios of 1–2. They are colorless and transparent. In CL images, most zircons show homogeneous, patchy, stripe or zoning texture and lack core-mantle structure, sharing most features of the zircons crystallized from mafic magma (Fig. 5). Twenty-two analyses were obtained and the age results are consistent within analytical errors. These zircons have variable Th and U contents with Th/U ratios ranging from 0.4 to 0.6. The weighted mean $^{206}Pb/^{238}U$ age of 481.4 ± 2.1 Ma ($N = 22$, MSWD = 0.68) (Fig. 7a) is interpreted as the crystallization age of the gabbros.

Zircons from the meta-rhyolite sample 2015D017 are of columnar forms, transparent and colorless, ranging from 80 μm to 150 μm in length with length/width ratios of 2–3. According to CL image features, almost all zircon grains display oscillatory zoning, sharing features of the zircons crystallized from silicic magmas. Some of them have core-mantle structure but the mantle part is too thin for a spot analysis (Fig. 5). Thirty-nine analyses were performed on zircons from this sample. They have Th ranging from 180 ppm to 852 ppm and U from 203 ppm to 1185 ppm with Th/U ratios between 0.6 and 0.9. All the analyses yield consistent $^{206}Pb/^{238}U$ ages with a weighted mean age of 480.7 ± 1.6 Ma (MSWD = 0.81) (Fig. 7b).

Zircons from the granodiorite sample 2015D016-1 are of columnar forms, transparent and colorless, ranging from 100 μm to 180 μm in length with length/width ratios of 2–3. Almost all zircon grains display oscillatory zoning in CL images. Cracks and metamictization can be seen in some zircons due to their high U contents and such zircons are avoided in analysis. Twenty analyses performed on this sample show that they have Th ranging from 180 ppm to 852 ppm and U from 203 ppm to 1185 ppm with Th/U ratios between 0.6 and 0.9. All the analyses yield consistent $^{206}Pb/^{238}U$ ages with a weighted mean age of 470.2 ± 2.2 Ma (MSWD = 0.36) (Fig. 7c). This age is interpreted as the crystallization age of the granodiorite.

Zircons from the gneissic granodiorite samples (2015D014) and the gneissic granite dyke sample (2015D015) have similar features. Most of the crystals are euhedral and range from 80 μm to 150 μm in length with length to width ratios of 1–3. They are transparent and colorless. Euhedral concentric zoning texture is commonly seen, sharing the typical features of the zircons crystallized from granitic magma. Some zircon grains show very thin bright rim in CL image possibly due to the overprinting of the tectonothermal event after their crystallization. Twenty-four and thirty-two analyses were conducted on 2015D014 and 2015D015, respectively. Both samples have comparable Th/U ratios ranging from 0.3 to 0.7 (mostly ~0.5) and yield concordant $^{206}Pb/^{238}U$ and $^{207}Pb/^{235}U$ ages. The mean $^{206}Pb/^{238}U$ age of the sample 2015D014 and 2015D015 are 445.0 ± 1.9 Ma (MSWD = 0.68) and 446.0 ± 1.6 Ma (MSWD = 0.93) (Fig. 8A and B), respectively, indicating coeval emplacement of the gneissic granodiorite and the gneissic granite dyke.

Most zircons grains from the amphibolite sample 2015D012-3 are round, transparent and colorless and are 50–120 μm long. Most of them are homogeneous and show relatively bright CL image, sharing features of metamorphic zircons and different from those of the zircons crystallized from mafic magma (Hoskin and Schaltegger, 2001). Thirty-two analyses were conducted on this sample. Their Th content ranges from 13 ppm to 196 ppm, U from

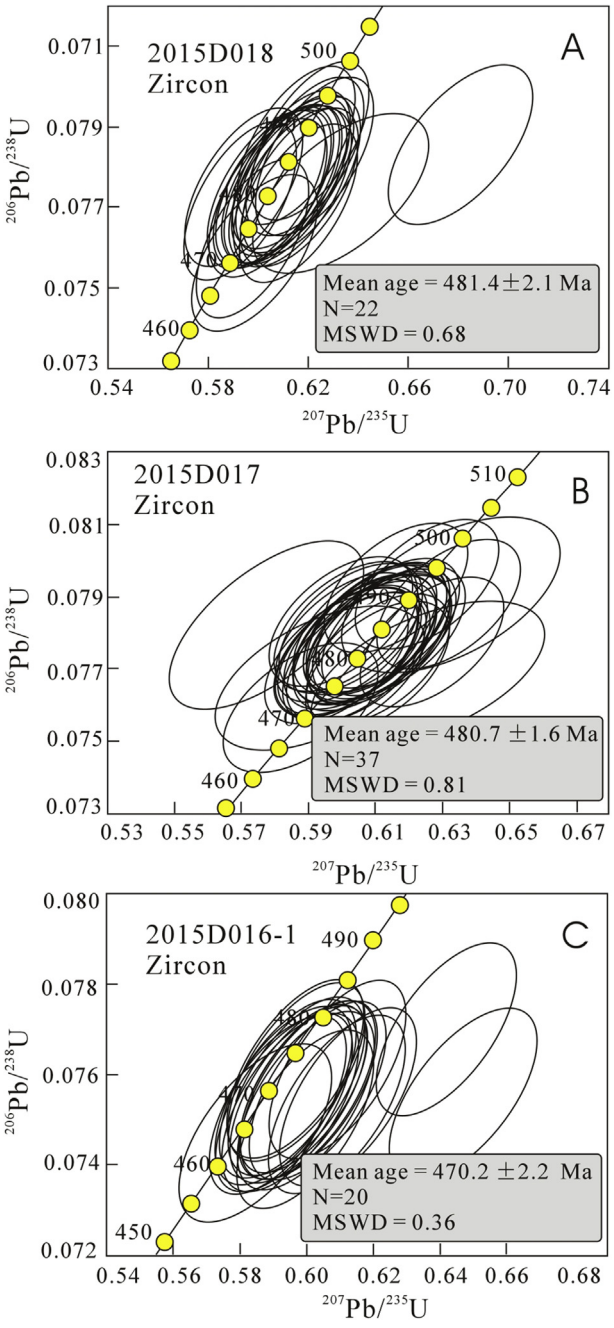

Figure 7. Concordia of the zircon U-Pb data of the gneissic granodiorite, granofels and altered gabbros from the Saitula Group (see details in the text).

110 ppm to 1351 ppm with Th/U ratios from 0.08 to 0.3 (mostly between 0.1 and 0.2). All the analyses yield concordant $^{206}Pb/^{238}U$ and $^{207}Pb/^{235}U$ ages with a weighted mean $^{206}Pb/^{238}U$ age of 442.8 ± 1.6 Ma (MSWD = 0.34) (Fig. 8C). This age was interpreted as the amphibolite-facies metamorphic age of the amphibolite.

Monazite grains from the biotite schist sample 2015D013 have anhedral morphology and are 100–150 μm long. In BSE images, most grains are homogenous with some showing patchy patterns with swirling bright and dark domains. The bright and dark domains are carefully avoided for analysis. Thirty analyses were conducted on this sample and almost all the analyses yield concordant $^{206}Pb/^{238}U$ and $^{207}Pb/^{235}U$ ages. Three spots (13.6, 13.9, 13.19) yield relatively juvenile concordant ages possibly due to

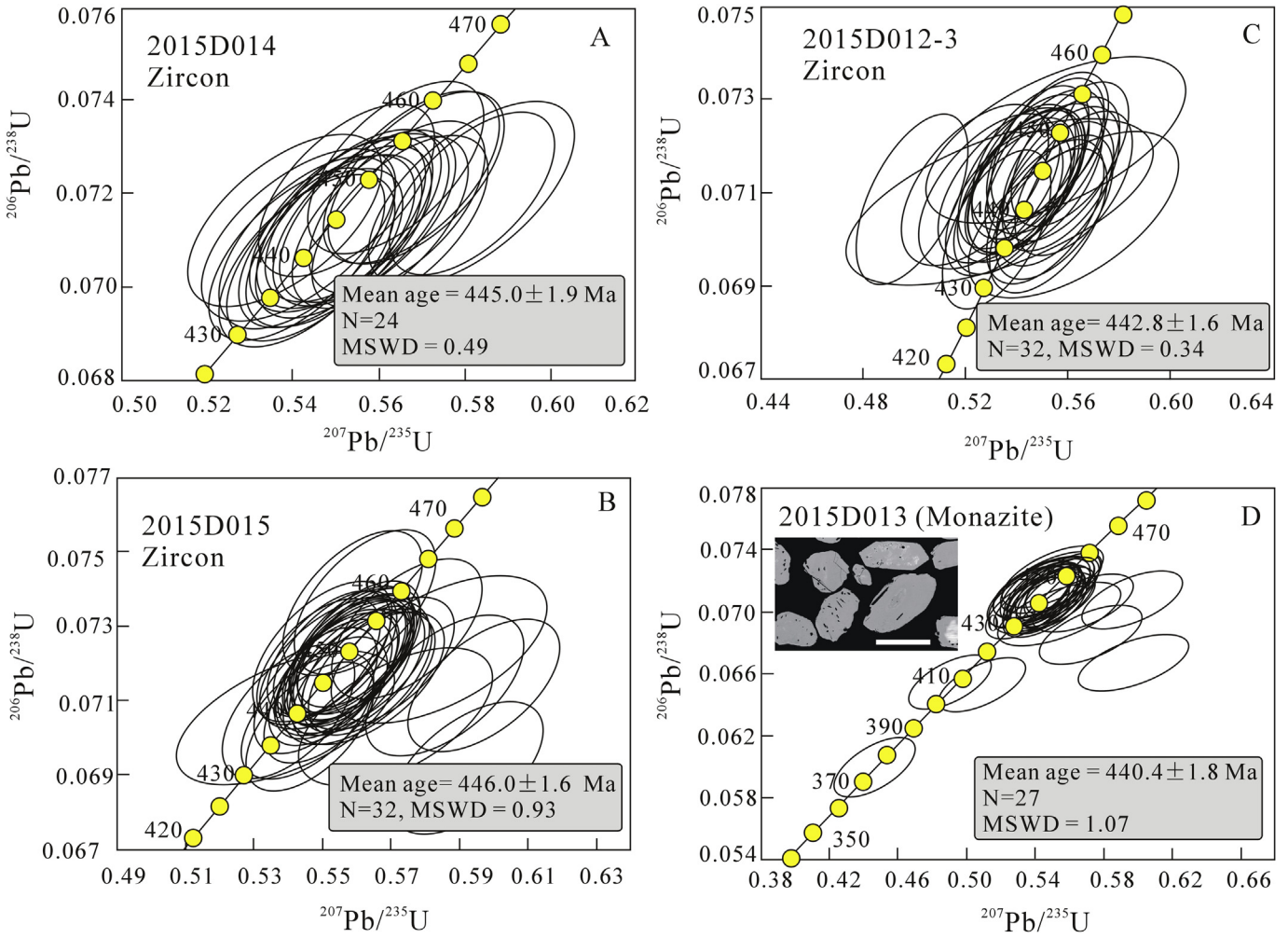

Figure 8. Concordia of the zircon U-Pb data of the gneissic granodiorite pluton and dyke (A, B), amphibolite (metamorphic origin zircons, C) and concordia of the monazites (D) from biotite schist collected from the Saitula Group (see details in the text).

variable involvement of the overgrowth monazites formed after the main metamorphic event. The other 27 analyses yield a mean $^{206}Pb/^{238}U$ ages of 440.4 ± 1.8 Ma (MSWD = 1.07) (Fig. 8D).

5.2. Zircon and monazite U-Pb ages of the Kangxiwa Group

Most zircons from the biotite plagioclase gneiss sample 2015D005-2 are generally colorless and some are slight pinkish. They are euhedral to sub-euhedral and are 80–150 μm long with length to width ratios of 1–2. They exhibit oscillatory zoning in CL images, sharing most features of the zircons crystallized from granitic magma. Twenty-seven analyses of 27 zircon grains yield concordant $^{206}Pb/^{238}U$ and $^{207}Pb/^{235}U$ ages ranging from 440 Ma to 2215 Ma (Supplementary Table 2). The weighted mean $^{206}Pb/^{238}U$ age of the seven youngest spots is 449.8 ± 2.6 Ma (MSWD = 1.2) (Fig. 9A).

The monazite grains from the leucogranite dyke (2015D010) are sub-euhedral to anhedral and are 80–150 μm long. In BSE images, all grains are homogenous. Monazites from the biotite schist sample (2015D005-3) share most features with those of the leucogranite except that most grains contain some fine inclusions (see inset of Fig. 9B and C). Thirty-two analyses were conducted on sample 2015D005-3 and sample 2015D010. According to the results (Supplementary Table 3), four spots from sample 2015D005-3 yield relatively juvenile $^{206}Pb/^{238}U$ ages possibly due to the overgrowth of the late tectonothermal event. The other analyses yield concordant $^{206}Pb/^{238}U$ and $^{207}Pb/^{235}U$ ages. The weighted mean $^{206}Pb/^{238}U$ ages of the two samples are 205.8 ± 1.2 Ma (MSWD = 2.0) for 2015D005-3 and 209.3 ± 1.3 Ma for 2015D010 (MSWD = 2.5) (Fig. 9B and C). These two ages were interpreted as the age of high-grade greenschist- to amphibolite-facies metamorphism for the Kangxiwa Group.

5.3. Zircon U-Pb ages of the Tianshuihai Group

Zircons from the two sandstone samples (2015D001 and 2015D019) are of columnar forms, transparent and colorless, ranging from 100 μm to 150 μm in length with length/width ratios of 1–3. Some zircons grains are oval or rounded, indicating their long-distance transport. According to CL image features, some zircon grains display oscillatory zoning whereas others display banded structure (Fig. 5). Forty-nine and eighty-seven analyses were performed on sample 2015D001 and 2015D019 respectively. As for the sample 2015D001, the zircons have Th ranging from 23 ppm to 613 ppm and U from 38 ppm to 614 ppm with Th/U ratios between 0.3 and 2.1 except for one spot (2015D00120) with Th/U ratio of 0.06. The analyses could be divided into three groups. Group 1 zircons yield nearly concordant ages with a mean $^{206}Pb/^{238}U$ age of 742.1 ± 4.2 Ma (N = 32, MSWD = 0.41) (Fig. 10). Group 2 zircons yield concordant $^{206}Pb/^{238}U$ and $^{207}Pb/^{235}U$ ages,

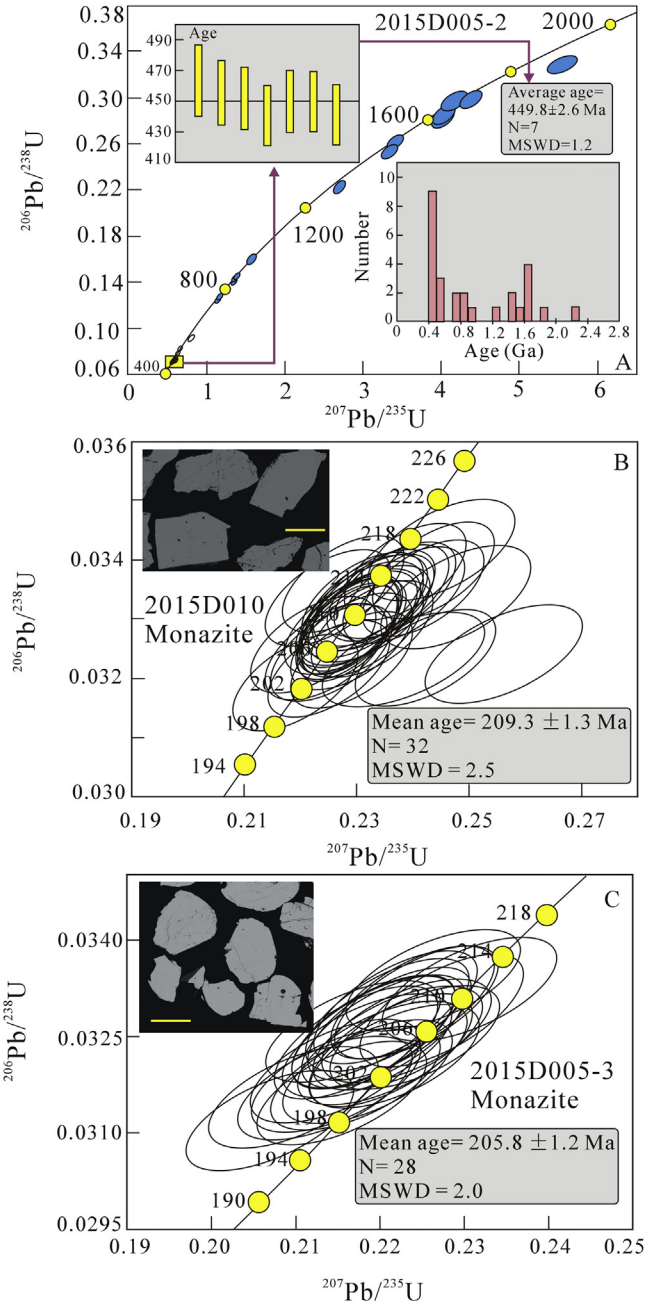

Figure 9. Concordia and the histogram of $^{206}Pb/^{238}U$ ages of the detrital zircons of the paragneiss samples from the Kangxiwa Group (A) and Concordia diagram of the monazites from the deformed leucogranite dyke and garnet biotite schist from the Kangixwa Group (B, C) (see details in the text).

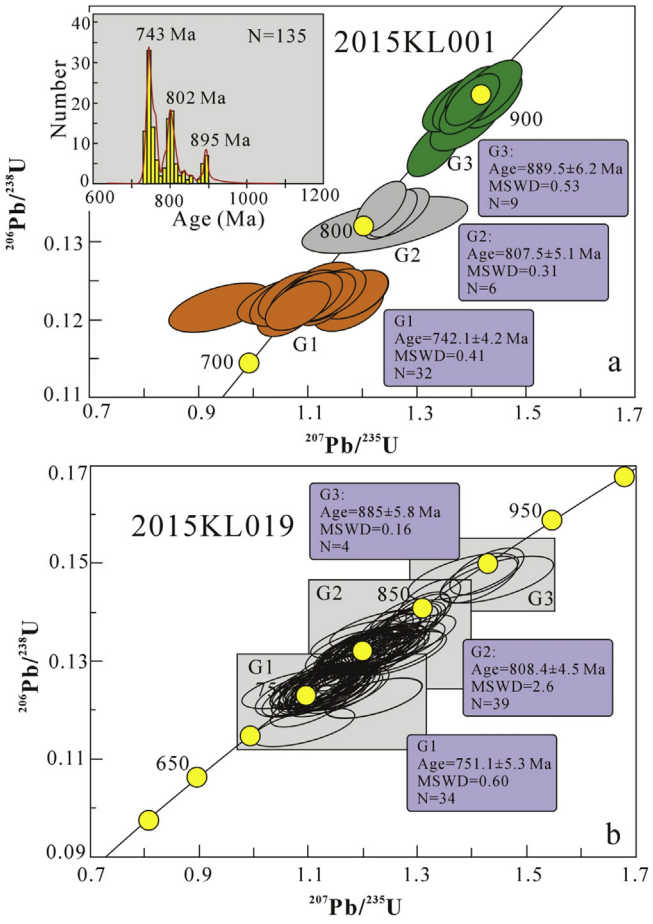

Figure 10. Concordia and the histogram of $^{206}Pb/^{238}U$ ages of the detrital zircons of the sandstone samples from the Tianshuihai Group.

forming a tight cluster at ca. 800 Ma with a mean $^{206}Pb/^{238}U$ age of 807.5 ± 5.1 Ma ($N = 6$, MSWD = 0.31) (Fig. 10). Group 3 zircons form a tight cluster with a mean $^{206}Pb/^{238}U$ age of 889.5 ± 6.2 Ma ($N = 11$, MSWD = 0.53) (Fig. 10a).

For sample 2015D019, most analyses yield concordant $^{206}Pb/^{238}U$ and $^{207}Pb/^{235}U$ ages ranging from 740 Ma to 890 Ma with three yielding early Precambrian ages (Supplementary Table 2 and Fig. 10b). Similar with the scenario of the sample 2015D001, the analyses could be broadly divided into three groups with mean $^{206}Pb/^{238}U$ age of 751.1 ± 5.3 Ma ($N = 34$, MSWD = 0.60), 808.4 ± 4.5 Ma ($N = 39$, MSWD = 2.6) and 885 ± 5.8 Ma ($N = 4$, MSWD = 0.16) (Fig. 10b). We combine all the age data in the insert of Fig. 10a that exhibits major peaks at ca. 743 Ma, 802 Ma and ca. 895 Ma. The youngest population (ca. 743 Ma) provides the maximum deposition age of the Tianshuihai Group (see following Discussions).

5.4. Zircon Hf isotope compositions

Five samples were selected for zircon Lu-Hf isotope analysis (Supplementary Table 3). Zircons from the 481 Ma altered gabbro sample (2015D018) have positive $\varepsilon_{Hf}(t = 481\ Ma)$ values ranging from 0.16 to 4.57 (Fig. 11a). The large range and non-Gaussian distribution pattern of positive $\varepsilon_{Hf}(t)$ suggest that the primitive magma originated from depleted mantle source with variable crustal contamination. The two coeval gneissic granite samples (2015D014 and 2015D015) have broadly similar Lu-Hf isotope compositions with $\varepsilon_{Hf}(t)$ ranging from −6.98 to 0.08, forming a broad Gaussian distribution pattern with a peak at ca. −4 (Fig. 11b). Most of the metamorphic zircons from the amphibolite sample (2015D012-2) have negative $\varepsilon_{Hf}(t)$ values ranging from −6.39 to 0.46 except for one zircon with a highly positive $\varepsilon_{Hf}(t)$ value of 7.32 (Fig. 11c). It is generally accepted that, for the in-situ zircon Hf isotope analysis by laser ablation method, the determined ^{176}Hf could be significantly affected by measured ^{176}Yb (Griffin et al., 2000; Vervoort et al., 2004; Wu et al., 2006). Due to its abnormally high ^{176}Yb, this spot is excluded for further discussions. Thus, the other 29 analyses form a good Gaussian distribution with a peak at ca. −3.1 (Fig. 11c). Three groups of zircons from the Tianshuihai Group have distinct Lu-Hf isotope compositions (Supplementary Table 3 and Fig. 11d). Note that the most juvenile zircon Group

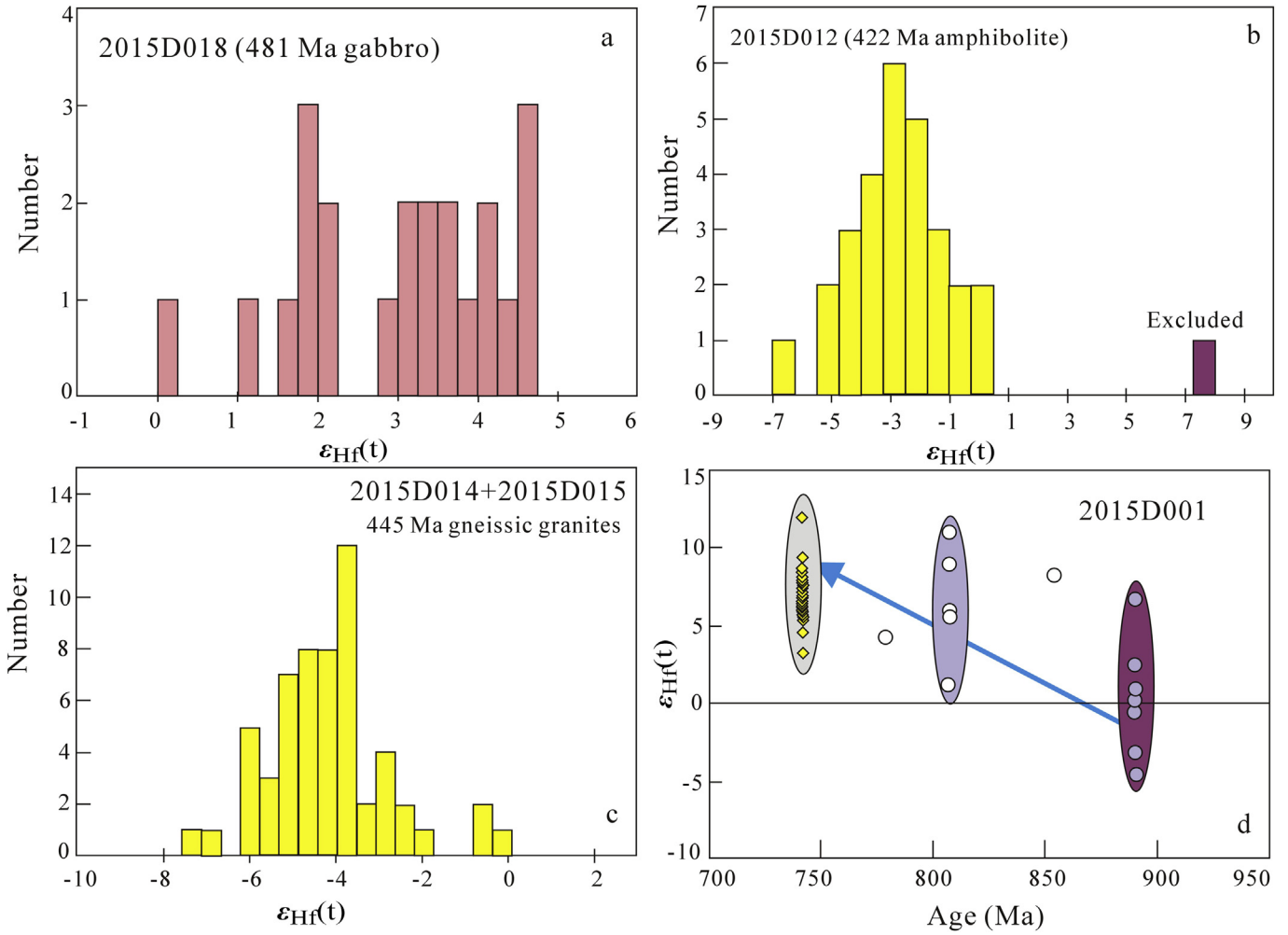

Figure 11. Histogram of the $\varepsilon_{Hf}(t)$ (a–c) and zircon U-Pb age vs. $\varepsilon_{Hf}(t)$ (d) diagrams of the representative rocks from the Saitula Group and the Tianshuihai Group (see details in the text).

(ca. 752 Ma) have significantly high $\varepsilon_{Hf}(t)$ and their $\varepsilon_{Hf}(t)$ values increase gradually from old population to young population (Fig. 11d). This scenario resembles that of the Neoproterozoic detrital zircons from South China (Li et al., 2014).

6. Discussions

6.1. Age of the Saitula Group

In the earlier Chinese geological maps, most high-grade metamorphic rocks were regarded as Precambrian basement due to the lack of reliable fossils or isotopic ages. For example, in South China, the amphibolite-(leptynite)-facies metamorphic rocks in Cathaysia were mapped as the Paleoproterozoic basement. As more and more in-situ zircon U-Pb ages are obtained, geologists have come to realize that the so-called Paleoproterozoic basement actually was deposited during the late Neoproterozoic to early Paleozoic. The amphibolite-(leptynite)-facies metamorphism took place at ca. 440–430 Ma because of the presence of abundant zircons of Pan-African ages (Wan et al., 2007, 2010; Li et al., 2014 and references therein).

Similar to the scenario in South China, the Saitula Group was considered as the Precambrian basement of the SKT drifted from the southern margin of the Tarim Block, on the basis of their amphibolite-facies metamorphism (e.g., Xinjiang BGMR, 1993; Han et al., 2004; Cui et al., 2006a, 2006b). According to field observations, the rock association of the Saitula Group differs from those of the Precambrian metamorphic rocks in NKT, such as the Heluositan Group, Kalakashi Group and Ailiankate Group (Fig. 2; Zhang et al., 2003, 2016b). Zircon U-Pb ages of the paragneiss from the Saitula Group provide the lower limit of its deposition age. In combination with the fact that voluminous ca. 500–450 Ma granites and 481 Ma gabbro intruded the Saitula Group, we suggest that the Saitula Group was deposited during 600–480 Ma or even slightly later, rather than Mesoproterozoic or Paleoproterozoic. It is interesting to note that a granofels sample yields a concordant age of ca. 481 Ma. As mentioned above, the protolith of the granofels was most likely rhyolite. Thus, it is inconsistent with the fact of 500–480 Ma granites intruding the Saitula Group. Because the Saitula Group was a huge accretionary wedge formed during the long-term southward subduction of the Proto–Tethys oceanic crust (beginning at ca. 530 Ma, see following discussions) and this granofels sample was collected at the upper part of the Saitula Group (nearby the marble member), we suggest that the deposition might occur slightly later than 480 Ma. During the subduction process, the intrusion of I-type granite could be coeval with the deposition of the volcano-sedimentary sequences. This scenario was also observed in the Altai orogenic belt (Xiao et al., 2009).

6.2. The age of the Kangxiwa Group

Petrographically, the Kangxiwa Group mainly consists of garnet-bearing para-gneiss and schist. Monazite U-Pb dating of the schist

and the deformed leucogranite dyke revealed that the high-grade greenschist- to amphibolite-facies metamorphism of the Kangxiwa Group took place at ca. 210–200 Ma. The youngest detrital zircon group yields a concordant age of ca. 450 Ma. Thus, the Kangxiwa Group was deposited after 450 Ma, possibly during the late Carboniferous to late Permian (Zhang et al., 2017a, b), rather than Mesoproterozoic as previously thought.

6.3. The age of the Tianshuihai Group

The deposition age of the Tianshuihai Group could be tightly constrained by the age of the youngest detrital zircon group and the age of the early Paleozoic gabbroic intrusion, *i.e.*, it should be younger than 743 Ma and older than 530 Ma (Hu et al., 2016). Thus, the Tianshuihai Group was deposited most likely during the late Neoproterozoic. Rock association of the Tianshuihai Group display the typical features of sedimentary sequences at passive continental margins, and the low-grade metamorphism of the Tianshuihai Group suggest that it had not been deeply buried during the evolution of the Tethys due to the possible presence of a basement beneath it (Zhang et al., 2018b).

6.4. Tectonic attribution of the Saitula Group and Kangxiwa Group

In line with the mineral compositions and textures, the precursors of some plagioclase-rich gneiss from the Saitula Group were likely volcaniclastic rocks. The common occurrence of amphibolite (meta-basalt), granofels (meta-rhyolite) interlayered within metamorphic immature clastic rocks (including volcaniclastic rocks) display typical features of the accretionary complex in the southern margin of the Altai orogenic belt (Xiao et al., 2009). On the other hand, we note that voluminous early Paleozoic granite-granodiorites and minor gabbros intruded the Saitula Group. Some of these granitic intrusions emplaced before 440 Ma exhibit gneissic structure and all of them show features typical of magmatic arc I-type granites (Pan, 1993, 1996; Yuan, 1999; Yuan et al., 2002; Cui et al., 2007a). Thus, the volcanic-sedimentary sequence of the Saitula Group and the intrusions constitute a typical early Paleozoic magmatic arc system.

In line with the rock association and its deposition age (late Paleozoic to early Mesozoic), the Kangxiwa Group most likely represents an overlying clastic sequence deposited after the amalgamation between NKT and TSHT. It was deeply buried during the early Mesozoic accretion process (210–200 Ma) and was exhumed possibly during the sinistral strike-slip motion of the Kangxiwa fault.

6.5. Tectonic attribution of the Tianshuihai terrane

The tectonic attribution of the Precambrian terranes distributed in the Tibet Plateau is unclear. Geologists have agreed that the Lhasa terrane, possibly including the South Qiangtang terrane, was drifted from the northern margin of the Gondwana due to their overprint by the Pan-African metamorphism (Zhu et al., 2011; Zhang et al., 2012). As for other terranes, studies in recent years revealed that most of them, such as the Qilian and Qaidam, share most Precambrian features with those of the Tarim and Yangtze (Song et al., 2010; Chen et al., 2012, 2013; Tung et al., 2012, 2013; Zhang et al., 2013). The age spectra of the detrital zircons and rock association of the Tianshuihai Group are similar to those of the late Neoproterozoic rocks in South China (Banxi Group and its equivalences, Meng et al., 2013; Song et al., 2017; Zhang et al., 2017). The lack of the Pan-African metamorphism in these terranes indicates that they were likely located at the northern fringe of the Gondwana and had never drifted far away from the India-Australia during the breakup of the Rodinia, which is entirely consistent with paleontology evidence (Metcalfe, 2011, 2013; Zhang et al., 2015; Metcalfe et al., 2017; Li et al., 2018). Thus, we suggest that the Tarim-Yangtze affinity type terranes (including the Qilian, Qaidam, Northern Qinling, Tianshuihai) could be located at the northern

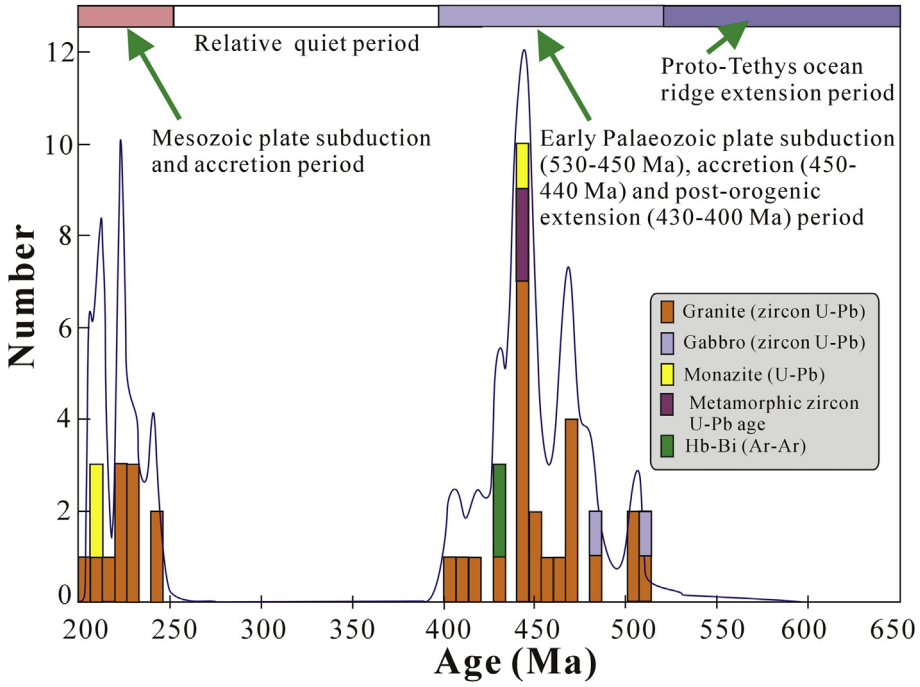

Figure 12. Histogram of the zircon U-Pb ages of the intrusive rocks, the metamorphic zircon and monazite U-Pb ages and mineral (hornblende, biotite) Ar-Ar ages for amphibolite-facies metamorphic rocks in SKT (data are from Cui et al., 2006a, 2007a,b; Zhang C.L. et al., 2007a; Zhang Y. et al., 2016a and references therein and this study).

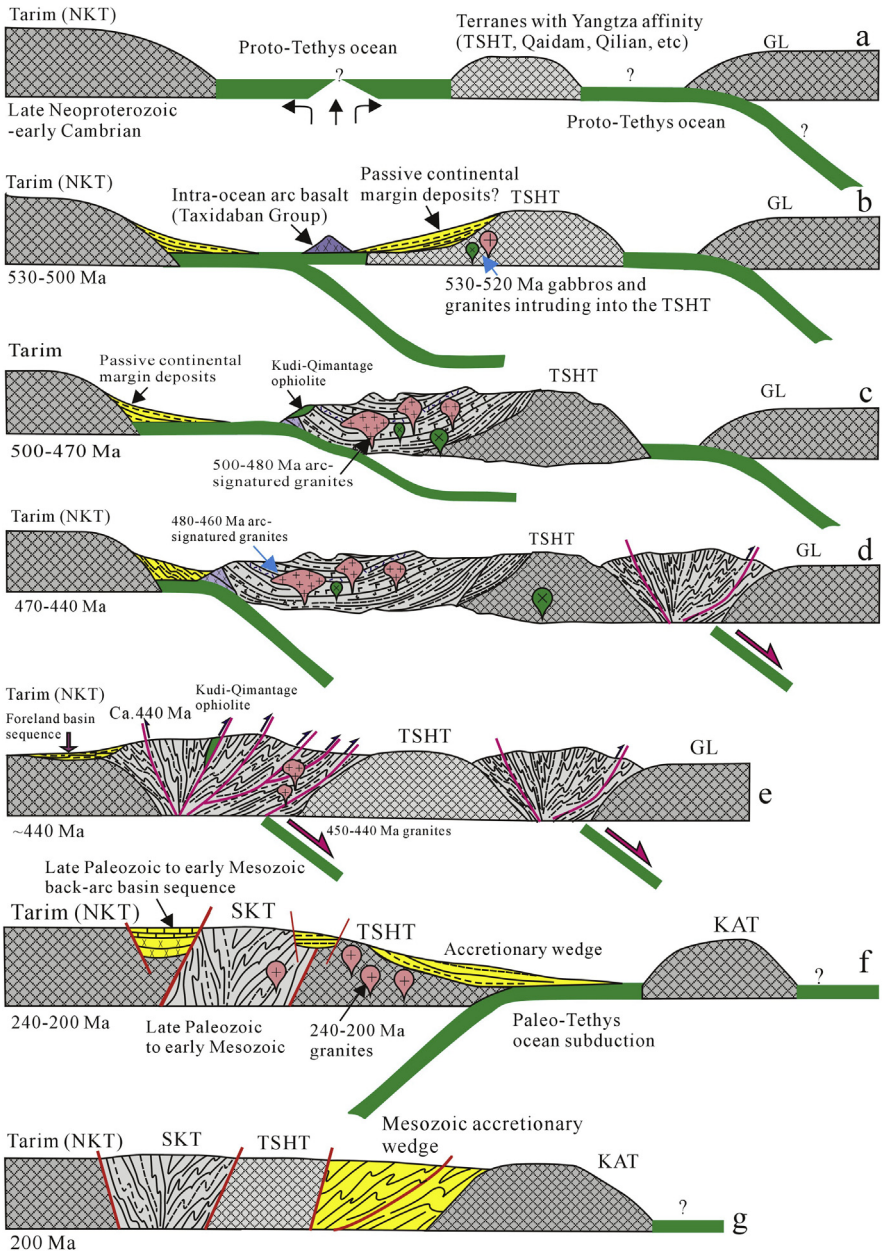

Figure 13. A schematic diagram to illustrate the tectonic evolution of the eastern section of WKOB (see details in text). Abbreviations: NKT—the North Kunlun terrane, SKT—the South Kunlun terrane, TSHT—the Tianshuihai terrane, KAT—the Karakorum terrane, GL—Gondwanaland.

margin of the Gondwana (Metcalfe, 2011, 2013; Metcalfe et al., 2017). This conclusion could well account for the commonly seen Pan-African detrital zircons from the Saitula Group.

6.6. Tectonic evolution of the WKOB

Geochronological data of the voluminous granites intruding the Saitula Group (Fig. 1b) (including minor mafic intrusions) revealed that the igneous activities in the eastern section of the WKOB could be divided into two distinct phases, i.e., 530–400 Ma and 240–200 Ma, which is consistent with metamorphic ages of the gneiss-schists in SKT (Fig. 12). According to the geochemical characteristics of the early Paleozoic granites, the 500–450 Ma granites show typical I-type features whereas the 430–400 Ma granites evolve from high Ba-Sr granite to A-type granite (Yuan, 1999; Yuan et al., 2002, 2005; Ye et al., 2008). Taken together, the plate subduction began slightly before 500 Ma and lasted till 450 Ma (Zhang et al., 2018a), and the accretion finished at ca. 440 Ma, according to the ca. 440 Ma amphibolite-facies metamorphism of the Saitula Group. This process was geodynamically related to the assemblage of the blocks in northern Tibet and eastern Asia (including the Tarim, Qaidam, South Qiangtang, Yangtze, Indochina, Sibumasu, etc.) to the northern margin of the Eastern Gondwana (Metcalfe, 2011, 2013; Diwu et al., 2014; Metcalfe et al., 2017; Li et al., 2018). In combination with the commonly seen early Paleozoic orogenic events along the northern Qaidam, Qilian, Qinling, Cathysia and terranes in Southeast Asia (Domeier and Torsvik, 2014; see details in Li et al., 2018), we suggest that the final assemblage of the above blocks to the Eastern Gondwana finished at 440–430 Ma.

We construct a cartoon model to illustrate the tectonic evolution of the eastern section of the WKOB. The prerequisite of this model is

that the Yangtze, Tarim, Qaidam, Qilian and TSHT were nearby the India-Australia during breakup of the Rodinia, and that shallow marine or limited ocean basin, *i.e.,* the Proto-Tethys ocean, was developed between the India-Australia and these terranes. Such a spatial pattern could guarantee the transport of the Pan-Africa detritus from Gondwana to the Tarim-Yangtze terranes (Fig. 13a). The southward Proto-Tethys ocean intra-ocean subduction possibly began at ca. 530 Ma, in line with the late Sinian to early Cambrian Taxidaban Group intra-ocean arc basalts and the ca. 530 Ma gabbro intruded into the Tianshuihai Group (Fig. 13b; Guo et al., 2002; Gao et al., 2015; Hu et al., 2016). This process also incubated the volcanic arc at the northern margin of the THST and this long-term subduction induced the large accretionary wedge at the northern margin of the THST (Fig. 13c and d). The ca. 510–490 Ma SSZ-type Kudi-Qimanyute ophiolite belt, mainly distributed at the northern margin of this accretionary wedge, most likely formed at a fore-arc environment, according to the geochemistry of the basalts that evolves from typical MORB to island-arc features (Han et al., 2002; Ji et al., 2004; Yuan et al., 2005). At ca. 440–450 Ma, NKT collided with TSHT, leading to the amalgamation between NKT and TSHT (Fig. 13e). Slab delamination induced the ca. 430–400 Ma post-orogenic igneous activities in the collision zone and the southern margin of the NKT (Ye et al., 2008). The orogenic events at this time were also well documented in Qilian, Qingling and Cathysia, indicating the final assemblage of the Tarim, Qaidam, Qilian, North Qinling and Yangtze to the northern margin of the Gondwana (Fig. 13e; Domeier and Torsvik, 2014; Cao et al., 2017; Metcalfe et al., 2017; Li et al., 2018).

We notice a relatively quiet period between 400 Ma and 250 Ma in the eastern section of WKOB as demonstrated by the absence of igneous activities and metamorphism (Fig. 12). The Devonian red molasse transformed into late Carboniferous - Permian passive continental margin sedimentary sequence. Since the late Paleozoic to early Mesozoic, the northward subduction of the Paleo-Tethys Ocean along the southern margin of TSHT generated the magmatic arc along the southern margin of SKT-TSHT and the back-arc volcanic sequence along the northern side of SKT (Fig. 13f, e.g., Domeier and Torsvik, 2014; Cao et al., 2017; Metcalfe et al., 2017; Li et al., 2018). The accretion of the Karakorum terrane to the NKT-SKT finished at ca. 200 Ma, according to the metamorphic ages of the Kangxiwa Group and the common Jurassic molasse unconformably in the SKT and the TSHT (Fig. 13g).

7. Conclusions

(1) The Saitula Group in NKT and the Tianshuhai Group in TSHT were deposited during the late Neoproterozoic to early Paleozoic, rather than Mesoproterozoic or Paleoproterozoic. The Kangxiwa Group was deposited during the late Paleozoic rather than Mesoproterozoic. Thus, our study does not favor the existence of a Precambrian basement in SKT.

(2) The Saitula Group was a large accretionary wedge between NKT and TSHT formed during the late Neoproterozoic to early Paleozoic. Southward subduction since Cambrian led to voluminous arc-signature granite emplacement in SKT. The collision between NKT and TSHT took place at ca. 440 Ma, leading to the accretion of Tarim, along with other terranes in the northern Tibet Plateau, to the northern margin of Gondwana.

(3) During the late Paleozoic to early Mesozoic, the northward subduction of the Paleo-Tethys ocean along the Hongshihu-Qiaoertianshan resulted in the formation of the voluminous arc-signature granites emplacements in southern part of the SKT-TSHT and the late Paleozoic to early Mesozoic accretionary wedge along the southern margin of the TSHT. The accretion was completed at ca. 200 Ma, which led to the closure of the Paleo-Tethys ocean between the TSHT and the Karakorum terrane.

Acknowledgments

We sincerely thank Mr. Jiang-Xin Wang for his help with the field work and supplying the 1/50000 geologic maps. We are grateful to Hong-Ying Zhou for his assistance with LA-ICP-MS zircon dating, and to Zhang Jian and Zhang Yong-Qing for their help with zircon Lu-Hf isotope analyses. Comments from Prof. Sanzhong Li and an anonymous reviewer greatly improved the quality of this paper. This project is funded by the National 305 Project of China (2018A03004-1, 2015BAB05B01-02) and the Fundamental Research Fund for Central Universities (B16020127).

Appendix A. Supplementary data

Supplementary data related to this article can be found at https://doi.org/10.1016/j.gsf.2018.05.006.

References

Andersen, T., 2002. Correction of common lead in U-Pb analyses that do not report ^{204}Pb. Chemical Geology 192, 59–79.

Cao, H.W., Huang, Y., Li, G.M., Zhang, L.K., Wu, J.Y., Dong, L., Dai, Z.W., Lu, L., 2017. Late Triassic sedimentary records in the northern Tethys Himalaya: tectonic link with Great India. Geoscience Frontiers 9 (1), 273–291. https://doi.org/10.1016/j.gsf.2017.04.001.

Chen, N.S., Zhang, L., Sun, M., Wang, Q.Y., Kusky, T.M., 2012. U-Pb and Hf isotopic compositions of detrital zircons from the paragneisses of the Quanji Massif, NW China: implications for its early tectonic evolutionary history. Journal of Asian Earth Sciences 54–55, 110–130.

Chen, N.S., Liao, F.X., Wang, L., Santosh, M., Sun, M., Wang, Q.Y., Mustafa, H.A., 2013. Late Paleoproterozoic multiple metamorphic events in the Quanji Massif: links with Tarim and North China cratons and implications for assembly of the Columbia supercontinent. Precambrian Research 228, 102–116.

Cui, J.T., Bian, X.W., Wang, G.B., 2006a. Geological composition and evolution of the West Kunlun. Geology of Shaanxi 24, 1–11 (in Chinese with English abstract).

Cui, J.T., Wang, J.C., Bian, X.W., Zhu, H.P., Yang, K.J., 2006b. Geological characteristics of Early Paleozoic amphibolite and tonalite in northern Kangxiwar, West Kunlun, China and their zircon SHRIMP U-Pb dating. Geological Bulletin of China 25, 1441–1449 (in Chinese with English abstract).

Cui, J.T., Bian, X.W., Wang, J.C., Yang, K.J., Zhu, H.P., Zhang, J.L., 2006c. Discovery of an unconformity between the Lower Silurian and Middle Devonian in the Tianshuihu area, southern Kangxiwar, West Kunlun, China. Geological Bulletin of China 25, 1437–1440 (in Chinese with English abstract).

Cui, J.T., Wang, J.C., Bian, X.W., Zhu, H.P., Luo, Q.Z., Yang, K.J., Wang, M.C., 2007a. Zircon SHRIMP U-Pb dating of early Paleozoic granite in the Mengguobao-Pushou area on the northern side of the Kangxiwa, West Kunlun. Geological Bulletin of China 26, 710–719 (in Chinese with English abstract).

Cui, J.T., Wang, J.C., Bian, X.W., Luo, Q.Z., Zhu, H.P., Wang, M.C., Chen, G.C., 2007b. Zircon SHRIMP U-Pb dating of the Dongbake gneissic tonalite in the northern Kangxiwa, West Kunlun. Geological Bulletin of China 26, 726–729 (in Chinese with English abstract).

Cui, Y.R., Zhou, H.Y., Geng, J.Z., Li, H.K., Li, H.M., 2012. In-situ LA-MC-ICP-MS U-Pb isotopic dating of monazite. Acta Geoscientica Sinica 33, 865–876 (in Chinese with English abstract).

Dewey, J.F., Shackleton, R.M., Chang, C., Sun, Y., 1988. The tectonic evolution of the Tibetan Plateau. Philosophical Transactions of the Royal Society of London A 327, 379–413.

Diwu, C.R., Sun, Y., Zhao, Y., Liu, B.X., Lai, S.C., 2014. Geochronological, geochemical, and Nd-Hf isotopic studies of the Qinling Complex, central China: implications for the evolutionary history of the North Qinling Orogenic Belt. Geoscience Frontiers 5, 499–513.

Domeier, M., Torsvik, T.H., 2014. Plate tectonics in the late Paleozoic. Geoscience Frontiers 5, 303–350.

Ducea, M.N., House, M.A., Kidder, S., 2003. Building the Pamirs: the view from the underside. Geology 31, 849–852.

Gao, X.F., Xiao, P.X., Kang, L., Ji, W.H., Yang, Z.C., 2015. Petrogenesis and tectonic implication of the A'qiang Mafic Lavas in the West Kunlun Orogen, NW China. Geotectonica et Metallogenia 39, 949–958 (in Chinese with English abstract).

Gao, R., Huang, H., Lu, D., 2000. Deep seismic reflection profile across the juncture zone between the Tarim basin and the West Kunlun mountains. Chinese Science Bulletin 45, 2281–2286.

Geng, J.Z., Li, H.K., Zhang, J., Zhang, Y.Q., 2011. Zircon Hf isotope analysis by means of LA-MC-ICP-MS. Geological Bulletin of China 30, 1508–1513 (in Chinese with English abstract).

Gibbons, A.D., Zahirovic, S., Muller, R.D., Whittaker, J.M., Yatheesh, V., 2015. A tectonic model reconciling evidence for the collisions between India, Eurasia

and intra-oceanic arcs of the central-eastern Tethys. Gondwana Research 28, 451–492.
Griffin, W.L., Pearson, N.J., Belousova, E., Jackson, S.E., Van Achterbergh, E., O'Reilly, S.Y., Shee, S.R., 2000. The Hf isotope composition of cratonic mantle: LAM-MC-ICPMS analysis of zircon megacrysts in kimberlites. Geochimica et Cosmochimica Acta 64, 133–147.
Guo, K.Y., Zhang, C.L., Zhao, Y., Dong, Y.G., Wang, A.G., 2002. Geochemistry of the Meso- to Neoproterozoic intra-oceanic arc volcanic rocks in the eastern segment of the West Kunlun orogenic belt. Geology in China 29, 161–166 (in Chinese with English abstract).
Han, F.L., Cui, J.T., Ji, W.H., Li, H.P., Hao, J.W., 2001. Discussion of orogenics of the West Kunlun mountains during the Caledonian orogeny. Geology of Shaanxi 19, 8–11 (in Chinese with English abstract).
Han, F.L., Cui, J.T., Ji, W.H., Li, H.P., Hao, J.W., 2002. Discovery of the Qimanyute ophiolite and its geological significance. Geological Bulletin of China 21, 573–578 (in Chinese with English abstract).
Han, F.L., Cui, J.T., Ji, W.H., Hao, J.W., Meng, Y., 2004. New results and major progress in the regional geological survey of the Yutian County and Bolike sheets. Geological Bulletin of China 23, 555–559 (in Chinese with English abstract).
Hou, K.J., Li, Y.H., Tian, Y.R., 2009. In situ U–Pb zircon dating using laser ablation multi ion counting-ICP-MS. Mineral Deposit 28, 481–492 (in Chinese with English abstract).
Hoskin, P.W., Schaltegger, U., 2001. The composition of zircon and igneous and metamorphic petrogenesis. Review in Mineralogy and Geochemistry 53, 25–104.
Hu, J., Wang, H., Huang, C.Y., Tong, L.X., Mu, S.L., Qiu, Z.W., 2016. Geological characteristics and age of the Dahongliutan Fe-ore deposit in the West Kunlun orogenic belt, Xinjiang, northwestern China. Journal of Asian Earth Sciences 116, 1–25.
Jackson, S.E., Pearson, N.J., Griffin, W.L., Belousova, E.A., 2004. The application of laser ablation-inductively coupled plasma-mass spectrometry (LA–ICP-MS) to in situ U–Pb zircon geochronology. Chemical Geology 211, 47–69.
Ji, W.H., Han, F.L., Wang, J.C., Zhang, J.L., 2004. Composition and geochemistry of the Subashi ophiolite mélange in the West Kunlun and its geological significance. Geological Bulletin of China 23, 1196–1201 (in Chinese with English abstract).
Ji, W.H., Li, R.S., Chen, S.J., He, S.P., Zhao, Z.M., Bian, X.W., Zhu, H.P., Cui, J.G., Ren, J.G., 2011. The discovery of Palaeoproterozoic volcanic rocks in the Bulunkuoler Group from the Tianshuihai Massif in Xinjiang of Northwest China and its geological significance. Science in China (Series D) 54, 61–72.
Jiang, C.F., Yang, J.S., Feng, B.G., Zhu, Z.Z., Zhao, M., Chai, Y.C., Shi, X.D., Wang, H.D., Hu, J.Q., 1992. Opening-closing tectonics of the Kunlun mountains. In: Geol. Memoirs., vol. 5. Geological Publishing House, Beijing, p. 224 (in Chinese with English abstract).
Jiang, Y.H., Jiang, S.Y., Ling, H.F., Zhou, X.R., Rui, X.J., Yang, W.Z., 2002. Petrology and geochemistry of shoshonitic plutons from the West Kunlun orogenic belt, northwestern Xinjiang, China: implications for granitoid geneses. Lithos 63, 165–187.
Jiang, Y.H., Ling, H.F., Jiang, S.Y., Fan, H.H., Shen, W.Z., Ni, P., 2005. Petrogenesis of a Late Jurassic peraluminous volcanic complex and its high-Mg, potassic, quenched enclaves at Xiangshan, Southeast China. Journal of Petrology 46, 1121–1154.
Jiang, Y.H., Liao, S.Y., Yang, W.Z., Shen, W.Z., 2008. An island arc origin of plagiogranites at Oytag, West Kunlun orogen, northwest China: SHRIMP zircon U–Pb chronology, elemental and Sr–Nd–Hf isotopic geochemistry and Paleozoic tectonic implications. Lithos 106, 323–335.
Jiang, Y.H., Jia, R.Y., Liu, Z., Liao, S.Y., Zhao, P., Zhou, Q., 2013. Origin of Middle Triassic high-K calc-alkaline granitoids and their potassic microgranular enclaves from the West Kunlun orogen, northwest China: a record of the closure of Paleo-Tethys. Lithos 156–159, 13–30.
Li, S.Z., Zhao, S.J., Liu, X., Cao, H., Yu, S., Li, X.Y., Somerville, I., Yu, S.Y., 2018. Closure of the Proto-Tethys Ocean and Early Paleozoic amalgamation of microcontinental blocks in East Asia. Earth-Science Reviews 186, 37–75. https://doi.org/10.1016/j.earscirev.2017.01.011 (in press).
Li, T.F., Zhang, J.X., 2014. Zircon LA-ICP-MS U-Pb ages of websterite and basalt in Kudi ophiolite and the implication, West Kunlun. Acta Petrologica Sinica 30, 2393–2401.
Li, X.H., Li, Z.X., Li, W.X., 2014. Detrital zircon U–Pb age and Hf isotope constrains on the generation and reworking of Precambrian continental crust in the Cathaysia Block, South China: a synthesis. Gondwana Research 25, 1202–1215.
Liu, Z., Jiang, Y., Jia, R., Zhao, P., Zhou, Q., 2015. Origin of Late Triassic high-K calc-alkaline granitoids and their potassic microgranular enclaves from the western Tibet Plateau, northwest China: implications for Paleo-Tethys evolution. Gondwana Research 27, 326–341.
Liu, J.G., Wang, J., 2016. Formation of A1-rich type podiform chromitites in the Kudi ophiolite. Acta Geologica Sinica 90, 1182–1194 (in Chinese with English abstract).
Ludwig, K.R., 2003. User's Manual for Isoplot 3.00: a Geochronological Toolkit for Microsoft Excel. Kenneth R. Ludwig.
Mahar, M.A., Mahéo, G., Goodell, P.C., Pavlis, T.L., 2014. Age and origin of post collision Baltoro granites, south Karakoram, North Pakistan: insights from in-situ U–Pb, Hf and oxygen isotopic record of zircons. Lithos 205, 341–358.
Matte, P., Tapponnier, P., Bourjot, L., Pan, Y., Wang, Y., 1992. Tectonics of Western Tibet, from the Kunlun to the Karakorum. International Symposium on the Karakorum and Kunlun Mountains, Abstracts, June 1992, Kashi, 36.
Matte, Ph, Tapponnier, P., Arnaud, N., Bourjot, L., Avouac, J.P., Vidal, Ph, Liu, Q., Pan, Y.S., Wang, Y., 1996. Tectonics of Western Tibet, between the Tarim and the Indus. Earth and Planetary Science Letters 142, 311–330.
Mattern, F., Schneider, W., 2000. Suturing of the Proto- and Paleo-Tethys oceans in the West Kunlun (Xijiang, China). Journal of Asian Earth Sciences 18, 637–650.
Mattern, F., Schneider, W., Li, Y., Li, X., 1996. A traverse through the West Kunlun (Xinjiang, China): tentative geodynamic implications for the Paleozoic and Mesozoic. Geologische Rundschau 85, 705–722.
Meng, Q.X., Zhang, J., Geng, J.Z., Zhang, C.L., Huang, W.C., 2013. Zircon U-Pb age and Hf isotope compositions of Lengjiaxi and Baxi Groups in middle Hunan Province: implications for the Neoproterozoic tectonic evolution in South China. Geology in China 40, 191–216 (in Chinese with English abstract).
Metcalfe, I., 2011. Palaeozoic-Mesozoic history of SE Asia. In: Hall, R., Cottam, M., Wilson, M. (Eds.), The SE Asian Gateway: History and Tectonics of Australia-Asia Collision, Geological Society of London Special Publications, vol. 355, pp. 7–35.
Metcalfe, I., 2013. Gondwana dispersion and Asian accretion: tectonic and palaeogeographic evolution of eastern Tethys. Journal of Asian Earth Sciences 66, 1–13.
Metcalfe, I., Henderson, C.M., Wakita, K., 2017. Lower Permian conodonts from Palaeo-Tethys Ocean Plate Stratigraphy in the Chiang Mai-Chiang Rai Suture Zone, northern Thailand. Gondwana Research 44, 54–66.
Pan, Y.S., 1990. Tectonic features and evolution of the West Kunlun Mountain region. Earth Sciences 3, 224–232 (in Chinese with English abstract).
Pan, Y.S., 1993. Proto-tethys Track in the West Kunlun, China, vol. 1. Seismological Press, Beijing, pp. 30–35.
Pan, Y.S., 1996. Geological Evolution of the Karakorum and Kunlun Mountains. Seismological Press, Beijing, pp. 34–78.
Pan, Y.S., Wang, Y., 1994. Discovery and evidence of the fifth Suture Zone of Qinghai–Tibetan Plateau. Acta Geophysica Sinica 37, 241–250 (in Chinese with English abstract).
Robinson, A.C., Yin, A., Manning, C.E., Harrison, T.M., Zhang, S.-H., Wang, X.-F., 2004. Tectonic evolution of the northeastern Pamir: constraints from the northern portion of the Cenozoic Kongur Shan extensional system. Geological Society of America Bulletin 116, 953–974.
Robinson, A.C., Yin, A., Manning, C.E., Harrison, T.M., Zhang, S.-H., Wang, X.F., 2007. Cenozoic evolution of the eastern Pamir: implications for strain-accommodation mechanisms at the western end of the Himalayan-Tibetan orogen. Geological Society of America Bulletin 119, 882–896.
Robinson, A.C., Ducea, M., Lapen, T.J., 2016. Detrital zircon and isotopic constraints on the crustal architecture and tectonic evolution of the northeastern Pamir. Tectonics 31, 1–16.
Song, S.G., Su, L., Li, X.H., Zhang, G.B., Niu, Y.L., Zhang, L.F., 2010. Tracing the 850-Ma continental flood basalts from a piece of subducted continental crust in the North Qaidam UHPM belt, NW China. Precambrian Research 183, 805–816.
Song, G.Y., Wang, X.Q., Shi, X.Y., Jiang, G.Q., 2017. New U-Pb age constraints on the upper Banxi Group and synchrony of the Sturtian glaciation in South China. Geoscience Frontiers 8, 1161–1173.
Tung, G.A., Yang, H.Y., Liu, D.Y., Zhang, J.X., Yang, H.J., Shau, Y.H., Tseng, C.Y., 2012. The amphibolite-facies metamorphosed mafic rocks from the Maxianshan area, Qilian block, NW China: a record of early Neoproterozoic arc magmatism. Journal of Asian Earth Sciences 46, 177–189.
Tung, G.A., Yang, H.Y., Liu, D.Y., Zhang, J.X., Yang, H.J., Shau, Y.H., Tseng, C.Y., 2013. The Neoproterozoic granitoids from the Qilian block, NW China: evidence for a link between the Qilian and South China blocks. Precambrian Research 235, 163–189.
Vervoort, J.D., Patchett, P.J., Soderlund, U., Baker, M., 2004. Isotopic composition of Yb and the determination of Lu concentrations and Lu/Hf ratios by isotopic dilution using MC-ICPMS. Geochemistry, Geophysics, Geosystems 5, 325–348.
Vavra, G., Schmid, R., Gebauer, D., 1999. Internal morphology, habit and U-Th-Pb microanalysis of amphibole to leptynite facies zircon: geochronology of the Ivren Zone (Southern Alps). Contributions to Mineralogy and Petrology 134, 380–404.
Wan, Y.S., Liu, D.Y., Jian, P., 2004. SHRIMP U-Pb dating of monazite and zircon. Chinese Science Bulletin 49, 1185–1190.
Wan, Y.S., Liu, D.Y., Xu, M., Zhuang, J., Song, B., Shi, Y., Du, Y.L., 2007. SHRIMP U–Pb zircon geochronology and geochemistry of metavolcanic and metasedimentary rocks in Northwestern Fujian, Cathaysia Block, China: tectonic implications and the need to redefine lithostratigraphic units. Gondwana Research 12, 166–183.
Wan, Y.S., Liu, D.Y., Wilde, S.M., Cao, J.J., Chen, B., Dong, C.Y., Song, B., Du, L.L., 2010. Evolution of the Yunkai terrane, South China: evidence from SHRIMP zircon U–Pb dating, geochemistry and Nd isotope. Journal of Asian Earth Sciences 37, 140–153.
Wang, C., Wang, Y.H., Liu, L., He, S.P., Li, R.S., Li, M., Yang, W.Q., Cao, Y.-T., Meert, J.G., Shi, C., 2014. The Paleoproterozoic magmatic–metamorphic events and cover sediments of the Tiekelik Belt and their tectonic implications for the southern margin of the Tarim Craton, northwestern China. Precambrian Research 254, 210–225.
Wang, Z.H., Sun, S., Li, J.L., Hou, Q.L., 2002. Petrogenesis of tholeiite associations in Kudi ophiolite (West Kunlun Mountains, northwestern China): implication for the evolution of back-arc basins. Contributions to Mineralogy and Petrology 143, 471–483.
Wang, Z.H., 2004. Tectonic evolution of the West Kunlun orogenic belt, western China. Journal of Asian Earth Sciences 24, 153–161.
Wang, Z.H., Sun, S., Hou, Q.L., Li, J.L., 2004. Effect of melt rock interaction on geochemistry in the Kudi ophiolite (West Kunlun Mountains, northwestern

China): implication for ophiolite origin. Earth and Planetary Science Letters 191, 33–48.
Whitehouse, M.J., Kamber, B.S., 2002. On the overabundance of light rare earth elements in terrestrial zircons and its implication for Earth's earliest magmatic differentiation. Earth and Planetary Science Letters 204, 333–346.
Wu, F.Y., Yang, Y.H., Xie, L.W., Yang, J.H., Xu, P., 2006. Hf isotopic compositions of the standard zircons and baddeleyites used in U–Pb geochronology. Chemical Geology 234, 105–126.
Xiao, W.J., Li, J.L., Hou, Q.L., Zhang, G.C., Chen, H.L., 1998. Structural style of the Southeastern West Kunlun and its implications for growing arc orogenesis. Acta Geophysica Sinica 41, 133–141.
Xiao, W.J., Windley, B.F., Chen, H.L., Zhang, G.C., Li, J.L., 2002a. Carboniferous-Triassic subduction and accretion in the West Kunlun, China: implications for the collisional and accretionary tectonics of the northern Tibetan plateau. Geology 30, 295–298.
Xiao, W.J., Windley, B.F., Hao, J., Li, J.L., 2002b. Arc-ophiolite obduction in the West Kunlun range (China): implications for the Palaeozoic evolution of central Asia. Journal of the Geological Society 159, 517–528.
Xiao, W.J., Windley, B.F., Liu, D.Y., Jian, P., Liu, C.Z., Yuan, C., Sun, M., 2005. Accretionary tectonics of the West Kunlun orogen, China: a Paleozoic-Early Mesozoic, long-lived active continental margin with implications for the growth of southern Eurasia. The Journal of Geology 113, 687–705.
Xiao, W.J., Windley, B.F., Yuan, C., Sun, M., Han, C.M., Lin, S.F., Chen, H.L., Yan, Q.R., Liu, D.Y., Qin, K.Z., Li, J.Y., Sun, S., 2009. Paleozoic multiple subduction-accretion process of the southern Altaids. American Journal of Science 309, 221–270.
Xinjiang BGMR, 1993. Regional Geology of the Xinjiang Uygur Autonomous Region. Geological Publishing House, Beijing, pp. 23–78 (in Chinese).
Xu, R.H., Zhang, Y.Q., Xie, Y.W., Chen, F.K., Vadal, P., Nicolas, A., Zhang, Q.D., Zhao, D.M., 1994. A discovery of an early Palaeozoic tectonomagmatic belt in the northern part of west Kunlun mountains. Scientia Geologica Sinica 4, 313–328 (in Chinese with English abstract).
Xu, R.H., Zhang, Y.Q., Xie, Y.W., Vadal, P., Nicolas, A., Zhang, Q.D., Zhao, D.M., 1996. Isotopic geochemistry of plutonic rocks. In: Pan, Y.S. (Ed.), Geologic Evolution of the Karakorum and Kunlun Mountains. Seismological Press, Beijing, pp. 137–186 (in Chinese).
Xu, Z.Q., He, B.Z., Zhang, C.L., Zhang, J.X., Wang, Z.M., Cai, Z.H., 2013. Tectonic framework and crustal evolution of the Precambrian basement of the Tarim Block in NW China: new geochronological evidence from deep drilling samples. Precambrian Research 235, 150–162.
Yang, J.S., Robinson, P.T., Jiang, C.F., Xu, Z.Q., 1996. Ophiolites of the Kunlun Mountains. China and their tectonic implications. Tectonophysics 258, 215–231.
Ye, H.M., Li, X.H., Li, Z.X., Zhang, C.L., 2008. Age and origin of the high Ba-Sr granitoids from northern Qinghai-Tibet Plateau: implications for the early Paleozoic tectonic evolution of the West Kunlun orogenic belt. Gondwana Research 13, 126–138.
Ye, X.T., Zhang, C.L., Santosh, M., Zhang, J., Fan, X.K., Zhang, J.J., 2016. Growth and evolution of Precambrian continental crust in the southwestern Tarim terrane: new evidence from the ca. 1.4 Ga A-type granites and Paleoproterozoic intrusive complex. Precambrian Research 275, 18–34.
Yin, J., Bian, Q., 1995. Geologic Map of the Karakorum–West Kunlun and Adjacent Regions (1:2M). Science Press, Beijing.
Yin, A., Harrison, T.M., 2000. Geologic evolution of the Himalayan–Tibetan orogen. Annual Review of Earth and Planetary Sciences 28, 211–280.
Yuan, C., 1999. Magmatism and Tectonic Evolution of the West Kunlun Mountains (PhD dissertation). University of Hongkong.
Yuan, C., Sun, M., Zhou, M.F., Zhou, H., Xiao, W.J., Li, J.L., 2002. Tectonic evolution of the West Kunlun: geochronologic and geochemical constraints from Kudi granitoids. International Geology Review 44, 653–669.
Yuan, C., Sun, M., Yang, J.S., Zhou, H., Zhou, M.F., 2004. Nb-depleted, Continental Rift-related Akaz Metavolcanic Rocks (West Kunlun): Implication for the Rifting of the Tarim Craton from Gondwana. In: Geological Society, London, Special Publications, vol. 226, pp. 131–143.
Yuan, C., Sun, M., Zhou, M.F., Xiao, W., Zhou, H., 2005. Geochemistry and petrogenesis of the Yishak Volcanic sequence, Kudi ophiolite, West Kunlun (NW China): implications for the magmatic evolution in a subduction zone environment. Contributions to Mineralogy and Petrology 150, 195–211.
Yuan, X.C., 1996. Geophysical Atlas of China. Geological Publishing House, Beijing, pp. 21–78 (in Chinese).
Zhang, Y.Q., Xie, Y.W., Xu, R.H., Vidal, P., Nicolas, A., 1996. Geologic Evolution of the Karakorum and Kunlun Mountains. In: Pan, Y.S. (Ed.). Seismological Press, Beijing, pp. 94–136 (in Chinese).
Zhang, C.L., Dong, Y.G., Zhao, Y., 2003. Geochemistry of Meso-Proterozoic volcanites in Western Kunlun: evidence for the plate tectonic evolution. Acta Geologica Sinica 77, 237–245.
Zhang, C.L., Yu, H.F., Shen, J.L., Dong, J.G., Ye, H.M., Guo, K.Y., 2004. Zircon SHRIMP age determination of the giant-crystal gabbro and basalt in Kuda, west Kunlun: dismembering of the Kuda ophiolite. Geological Review 50, 639–643 (in Chinese with English abstract).
Zhang, C.L., Yu, H.M., Wang, A.G., Guo, K.Y., 2005. Dating of Triassic granites in the West Kunlun Mountains and its tectonic significance. Acta Geologica Sinica 79, 645–652 (in Chinese with English abstract).
Zhang, C.L., Yu, H.F., Ye, H.M., Wang, A.G., 2006. Aoyitake plagiogranite in western Tarim Block, NW China: age, geochemistry, petrogenesis and its tectonic implications. Science in China (Series D) 49, 1121–1134.
Zhang, C.L., Lu, S.N., Yu, H.F., Ye, H.M., 2007a. Tectonic evolution of Western Orogenic belt: evidences from zircon SHRIMP and LA-ICP-MS U-Pb ages. Science in China (Series D) 50, 1–12.
Zhang, C.L., Li, Z.X., Li, X.H., Ye, H.M., 2007b. Early Palaeoproterozoic high-K intrusive complex in southwestern Tarim Block, NW China: age, geochemistry and implications for the Paleoproterozoic tectonic evolution of Tarim. Gondwana Research 12, 101–112.
Zhang, Z.M., Dong, X., Santosh, M., Liu, F., Wang, W., Yiu, F., He, Z.Y., Shen, K., 2012. Petrology and geochronology of the Namche Barwa Complex in the eastern Himalayan syntaxis, Tibet: constraints on the origin and evolution of the northeastern margin of the Indian Craton. Gondwana Research 21, 123–137.
Zhang, C.L., Zou, H.B., Li, H.K., Wang, H.Y., 2013. Tectonic framework and evolution of the Tarim Block in NW China. Gondwana Research 23, 1306–1315.
Zhang, C.L., Santosh, M., Zhu, Q.B., Chen, X.Y., Huang, W.C., 2015. The Gondwana connection of South China: evidence from monazite and zircon geochronology in the Cathaysia Block. Gondwana Research 28, 1137–1151.
Zhang, Y., Niu, Y.L., Hu, Y., Liu, J.J., Ye, L., Kong, J.J., Duan, M., 2016a. The syncollisional granitoid magmatism and continental crust growth in the West Kunlun Orogen, China – evidence from geochronology and geochemistry of the Arkarz pluton. Lithos 245, 191–204.
Zhang, C.L., Ye, X.T., Zou, H.B., Chen, X.Y., 2016b. Neoproterozoic sedimentary basin evolution in southwestern Tarim, NW China: new evidence from field observations, detrital zircon U-Pb ages and Hf isotope compositions. Precambrian Research 280, 31–45.
Zhang, L., Long, X.P., Zhang, R., Dong, Y.P., Yuan, C., Xiao, W.J., Wang, Y.J., 2017. Source characteristics and provenance of metasedimentary rocks from the Kangxiwa Group in the Western Kunlun Orogenic Belt, NW China: implications for tectonic setting and crustal growth. Gondwana Research 46, 43–56.
Zhang, C.L., Zou, H.B., Ye, X.T., Chen, X.Y., 2018a. Tectonic evolution of the NE section of the Pamir Plateau: new evidence from field observations and zircon U-Pb geochronology. Tectonophysics 723, 27–40.
Zhang, C.L., Zou, H.B., Ye, X.T., Chen, X.Y., 2018b. A newly identified Precambrian terrane at the Pamir Plateau: the Archean basement and Neoproterozoic granitic intrusions. Precambrian Research 304, 73–87.
Zhang, Z., Xiao, X., Wang, J., Wang, Y., Kusky, T.M., 2008. Post-collisional Plio–Pleistocene shoshonitic volcanism in the West Kunlun Mountains, NW China: geochemical constraints on mantle source characteristics and petrogenesis. Journal of Asian Earth Sciences 31, 379–403.
Zhou, H., Li, J.L., Hou, Q.L., Xiao, W.J., Chen, H.H., 1999. A large-scale ductile shear zone in Kudi, West Kunlun. Chinese Science Bulletin 142, 1774–1776.
Zhou, H., Chu, Z.Y., Li, J.L., Hou, Q.L., Wang, Z.H., Fang, A.M., 2000. $^{40}Ar/^{39}Ar$ dating of ductile shear zone in Kuda, west Kunlun, Xinjiang. Scientia Geologica Sinica 35, 233–239 (in Chinese with English abstract).
Zhu, W.B., Zheng, B.H., Shu, L.S., Ma, D.S., Wu, H.L., Li, Y.X., Huang, W.T., Yu, J.J., 2011. Neoproterozoic tectonic evolution of the Precambrian Aksu blueschist terrane, northwestern Tarim, China: insight from LA-ICP-MS zircon U-Pb ages and geochemical data. Precambrian Research 185, 215–230.